TAMPERE UNIVERSITY OF TECHNOLOGY

ALEKSI OJALA

MODELLING OF EXTENDED ENDPLATE CONNECTION IN AMBIENT TEMPERATURES AND FIRE

Master of Science Thesis

Examiner: Professor Markku Heinisuo
Examiner and subject approved at Faculty of Built Environment council meeting on 03 of March 2010

ABSTRACT

TAMPERE UNIVERSITY OF TECHNOLOGY
Master's Degree Programme in Civil Engineering
OJALA, ALEKSI: Modelling of extended endplate connection in ambient temperatures and fire
Master of Science Thesis, 52 pages, 2 appendix pages.
March 2010
Major: Structural Engineering
Examiners: Professor Markku Heinisuo, M.Sc. Henri Perttola
Keywords: FEM, Steel structures, Extended endplate, component method, fire

In this study simulations were done to acquire data on 3D and fire behaviour of an extended endplate joint, and to evaluate the suitability of the FEM software SAFIR on modelling 3D beam to column joints. Three cases were modelled, two with simplified joints in ambient temperature, and one with half of a frame modelled in fire condition. The simple joints were loaded with moment to strong (vertical) direction, and moment to the weak (horizontal) direction. The half frame was loaded with a constant load and subjected to a standard fire. The results of these simulations were compared with the component method calculations according standard EN 1993-1-8 (2005) for simplified model, and with the test data from the test done at the University of Manchester (Wang et al 2008) for the half frame model. Notes on modelling and sources of error are discussed in conclusions.

TIIVISTELMÄ

TAMPEREEN TEKNILLINEN YLIOPISTO
Rakennustekniikan koulutusohjelma
OJALA ALEKSI: Jatketun päätylevyliitoksen mallinnus huoneenlämmössä ja tulipalossa
Diplomityö, 52 sivua, 2 liitesivua
Maaliskuu 2010
Pääaine: Rakennesuunnittelu
Tarkastaja: Professori Markku Heinisuo, DI Henri Perttola
Avainsanat: FEM, Teräsrakenteet, jatkettu päätylevyliitos, tulipalo, komponenttimenetelmä

Tutkimuksessa simuloitiin jatkettua päätylevyliitosta huoneenlämmössä, sekä altistettuna standardipalolle. Tavoitteena oli kerätä tietoa liitoksen 3D–käyttäytymisestä, sekä käyttäytymisestä palolle altistettuna. Tutkimuksen toinen tavoite oli arvioida FEM -ohjelman SAFIR soveltuvuutta liitosten 3D-mallinnukseen. Tutkimuksessa mallinnettiin yhteensä kolme tapausta, kaksi yksinkertaistetulla mallilla huoneenlämmössä ja yksi mallintamalla puolikas kehästä altistettuna standardipalolle. Yksinkertaistetut liitokset oli kuormitettu pistevoimalla aikaansaadulla momentilla vahvaan, sekä heikkoon suuntaan. Pistevoima kasvoi yksinkertaistetussa mallissa ajan funktiona murtoon asti. Puolikas kehä oli kuormitettu vakiolla pistekuormalla. Yksinkertaistetun mallin simulaatioiden tuloksia verrattiin Eurokoodin (EN 1993-1-8 2005) mukaan suoritettuihin komponenttilaskelmiin, ja puolikkaan kehän tuloksia Manchesterin yliopistossa suoritettuihin polttokokeisiin (Wang et al 2008) Tehdyt huomiot mallinnuksen ongelmista ja virhelähteistä esitetään johtopäätelmissä.

PREFACE

This study was done at Tampere University of Technology, Department of Structural Engineering, in the Research Centre of Metal Structures. The study was guided and supervised by professor Markku Heinisuo.

I would like to thank professor Markku Heinisuo for all the guidance and time he has given to my work, and for supervising my work. I also thank Henri Perttola for being the other examiner for this study, and also the whole team at the Centre of Metal Structures for support and for the dialogue we have been having during this study. I also thank the colleagues sharing the room with me, for a pleasant and inspiring environment to work in.

I also want to thank my family and friends for the support they have given me during this study, and the duration of my life so far. The last but not in any way least is my partner Juuli, for patience, support and everything else.

In Tampere, 8.4.2010

Aleksi Ojala

TABLE OF CONTENTS

TERMS AND NOMENCLATURE

Basic component	Single part of the joint that contributes to one or more of its structural properties.
Component method	Mechanical model for calculating joint behaviour.
Connection	Location where one or more structural element meet.
Equivalent T-stub	Method for calculating limiting yield mechanism of end-plate.
Failure mode	Failure mechanism associated with the equivalent T-stub.
Joint	Zone where two or more structural members are connected.
Joint behaviour	Resistance, stiffness and ductility of a joint.
Yield mechanism	Failure mechanism associated with the actual endplate.
A_f	Area of compressed flange in weak direction bending
A_s	Tensile stress area of a bolt
$F_{t.Rd}$	Design tensile resistance for a bolt
$F_{t.wb.Rd}$	Beam web tension resistance
$F_{c,Rd}$	Beam flange compression resistance
$M_{c,Rd}$	Beam plastic moment resistance
$M_{pl.i.Rd}$	Design plastic moment resistance of the failure mode *i*.
W_{pl}	Plastic moment resistance
$M_{j,Rd}$	Design moment resistance of the joint
L_b	Elongation length of the bolt
$b_{eff,t,wb}$	Effective width of beam web in tension
b_p	Endplate width
e	Horizontal distance from bolt to the edge of endplate
e_x	Vertical distance from bolt row 1 to edge of endplate
f_{ub}	Ultimate strength of the bolt
f_y	Yield limit
h	Beam height
h_r	Distance of bolt row from center of compression
k_2	Factor for taking into account the type of the bolt
$l_{eff.i}$	Effective length of equivalent T-stub for i:th failure mode

$l_{eff.cp}$	Effective length of equivalent T-stub for circular yield pattern
$l_{eff.nc}$	Effective length of equivalent T-stub for noncircular yield pattern
m	Horizontal distance from bolt center to beam web
m_2	Distance from upper flange to bolt row 2
m_3	Distance from lower flange to bolt row 3
m_x	Distance from upper flange to bolt row 1, extended part of endplate
n	Shortest horizontal distance from bolt center to endplate edge (e_{min})
p	Bolt row distance between the beam flanges
t_{fb}	Thickness of the beam flange
t_p	Thickness of the endplate
t_{wb}	Thickness of the beam web
w	Distance of the bolt center points, extended endplate
α	Factor for taking into account the effect of stiffeners on the yield mechanisms in endplate
λ_1	Variable for defining α
λ_2	Variable for defining α
γ_{M0}	Partial safety factor for ductile members
γ_{M2}	Partial safety factor for brittle members

1. INTRODUCTION

The joints in steel frames are traditionally considered either pinned or rigid in design. It is however clear, that the actual joint action is in most of the cases neither absolutely rigid nor pinned, but semi-rigid. The assumption is done for simplifying the calculations, but has disadvantages when considering both safety and economy of the structure. For example, cross sections with less moment capacity can be used in the ultimate limit state because of the smaller sagging moment in the mid span, and in the serviceability limit state the rotational stiffness of the joint reduces midpoint deflections significantly, allowing for more economic selection of cross section, especially in long span designs (Burgess 2008).

The obvious advantages of modeling the actual joint behaviour has created research efforts starting from 1970's to create consistent methodology to represent the behaviour of steel joints (Simoẽs Da Silva 2008). Early efforts were directed to represent the moment-rotation curve by mathematical models fitted to experimental data, or curve fit models (Burgess 2008). The disadvantage of this approach is the need of experimental results for each joint type to fit the model to. Expanding curve fit models to for e.g. fire conditions would lead to vast amounts of test setups and experiments with different axial force, moment and temperature combinations, rendering the curve fit approach unpractical in practice (Burgess 2008). Early efforts before emerging of, more practical, mechanical models are summarized comprehensively by Nethercot and Zandonini (1989) and are not in the scope of this study.

Component method is a mechanical model first introduced for 2D and ambient conditions by Tschemmernegg et al (1987). The idea of the method is to present different zones in the joint with non-linear springs and rigid links and analyze these zones individually. The resistance and rotational stiffness of the full joint can be then modelled by combining the effects of these different zones. Component method was included in the Eurocode EC3-1-8 (EN 1993-1-8 2005) as the method of designing steel joints. Component method allows taking the rotational capacity of semi-rigid joints in to account in the global analysis, allowing more realistic design. In addition, ductility, or the rotational capacity, of the joints can be calculated. The component method is general, and can thus be applied to many different cases, provided that the required components are available.

In the early stages, the method was only suitable for 2D cases because of the lack of required elements to model complex interactions present in 3D loading. Eurocode also did not require additional checks on joint robustness in fire conditions as recently as in the pre standard ENV-1993-1-2 (1995). The reason to this was that the increased bulk

(mass compared to the surface area) of the joint, compared to adjoining members was considered enough to provide the needed resistance (Simoẽs Da Silva 2008). However Findings of Cardington fire tests (Al-Jabri 1999) and catastrophic events of WTC 7 in 2001 (NCSTAR 1-9 2008), have raised concerns about the robustness of steel joints in fire.

Research has been done during recent years by many research groups around the world on the design of steel joints under fire conditions and under 3D loads. In fire conditions, the assumptions made when determining the static model of the structure may change, for example, thermal expansion can cause both compressive and tensile forces in the joint, depending on the phase of the fire, and collapse of parts of the structure may change the behaviour of the structure completely.

The application of component method to more complex, 3D, situations requires new components to be created. In EN-1993-1-8 (2005) 21 different components are presented to base the calculations on. These components are all for strong axis bending, and not applicable e.g. for cases when bending occurs with inclination. It is therefore crucial to create new components for 3D cases.

There is however a lack of data to base the new components on. Thus new tests and FEM-models of different cases are needed, to compare and, eventually, to validate the new components to. In this study, two bending moment cases for an extended endplate connection are simulated. The goal of the study is to get results for the moment resistance of the joint. The rotational stiffness is not considered in this study. The cases studied are bending to the strong axis direction $M_{y,}$ and to the weak axis (horizontal) direction $M_{z.}$ The displacements of the beam end at endplate are another matter studied in the test, as they give information about the deformations of the endplate. This information will help in the work on defining additional components for 3D-loading cases. The results are compared to calculations done by the component method according to the standard EN-1993-1-8 (2005)

The joint configuration modelled in this study was used in fire tests at the University of Manchester (Wang et al 2008). In the tests, the joint was loaded with an even moment load, and subjected to fire following the ISO-834 fire curve. The secondary objective of this study was to model the test, to gain knowledge on the modeling of whole structures in fire. The goal of this part of the modeling was to compare the temperatures when the collapse initiated.

The finite element method (FEM) program SAFIR was used for modelling both cases. SAFIR is a program developed at the University of Liege, for both thermal and structural analysis of structures (Franssen 2007). In addition to the simulations and their findings, experience on modelling with SAFIR and its suitability for this type of modelling was also a goal in this study.

2. COMPONENT METHOD

2.1. Component Method

The joint is represented by a set of linear springs in the component method included in EN-1993-1-8 (2005). After combining the effect of these different springs, or components, the resistance and rotational stiffness of the joint can be calculated. The basic components for modelling joints are presented in EN 1993-1-8 (2005). The method has been extended to cases with non-linear springs (Del Savio et al. 2009).

2.1.1. Terminology

In the component method the *basic component* means one single part of the joint that contributes to one or more of its structural properties, for example bolt or weld. *Connection* is the location where two or more structural elements meet, and is an assembly of the *basic components* that are required to represent the behaviour during the transfer of relevant forces and moments in the connection. The *joint* is the zone where two or more members are interconnected. E.g. beam-to-column *joint* consists of the column web shear *component* and one *connection,* see figure 2.1.

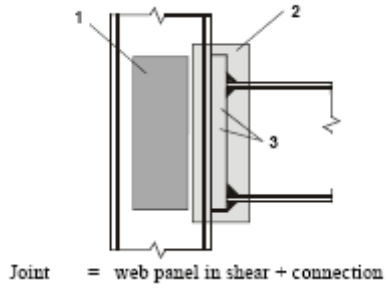

Figure 2.1 Single sided joint configuration:, 1. web panel in shear, 2. connection, 3. components (figure from EN-1993-1-8 2005)

The joint behaviour means the resistance, stiffness and ductility of the joint.

The equivalent T-stub approach is used when defining the limiting yield mechanisms for example for the endplate. The T-stub has different *failure modes*, while the actual endplate has *yield mechanisms*. The failure modes for equivalent T-stub are yield of flange and bolts together, total yield of flange and the yield of bolts only. (EN 1993-1-8 2005). The yield mechanisms can be either for individual bolts, or for bolts acting in a group. The yield lines depend on the geometry of the joint, and EN-1993-1-8 (2005) gives the equations to calculate the length of the equivalent T-stub for each of these

mechanisms. The yield lines given in eurocode are based on studies made in the Netherlands (Zoetemeijer 1974). The yield lines for the cases studied in this paper are presented in figures 2.2 – 2.5.

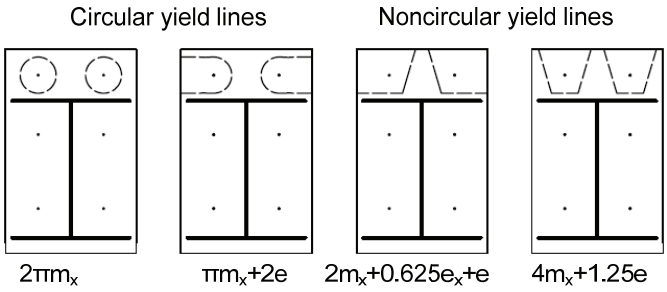

Figure 2.2 Yield mechanisms for individual bolts on extended part of the endplate

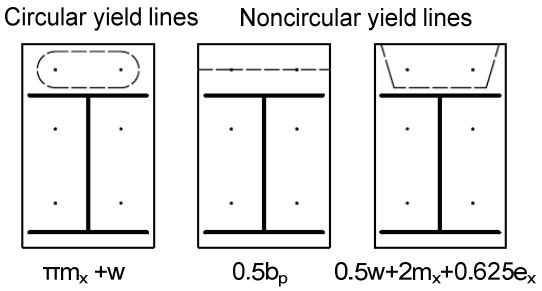

Figure 2.3 Yield mechanisms for bolts on extended part of the endplate, bolts acting as a group

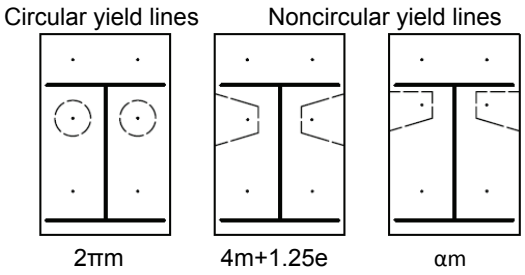

Figure 2.4 Yield mechanisms for individual bolts between beam flanges

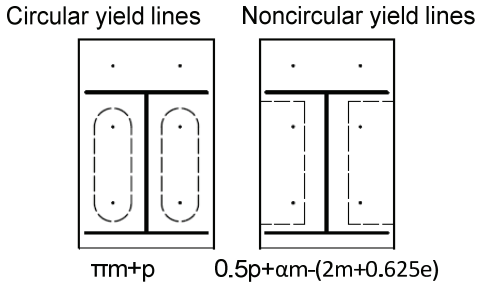

Figure 2.5 Yield mechanisms for bolts acting as a group between beam flanges

2.2. Cases Studied

A simplified connection following tests at the University of Manchester (Wang et al 2008) was modelled with the component method. The column was left out of the model

as it was very strong compared to the beam in the tests and only minor deformations occurred in the column, see figure 2.6.

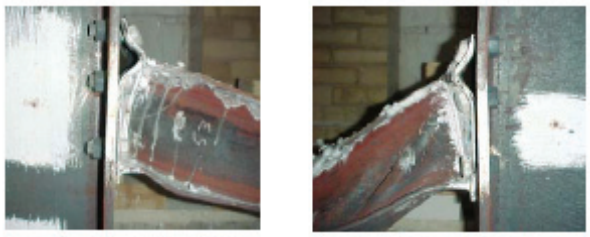

Figure 2.6 The endplate and beam deformation in the tests (Wang et al 2008)

The fact that the column remains almost completely undeformed can be observed from figure 2.6. The endplate bends significantly. In addition, the buckling of the lower flange occurred in the test and is also visible form the figure 2.6.

The calculations were done for two different loading cases, moment M_y to the strong direction of the joint and moment M_z to the weak direction of the joint, see figure 2.7 for idealization of the joint. The scope of this study was limited only to the moment resistance of the joints, as the simplified FEM model used was not considered suitable to study e.g. rotational stiffness.

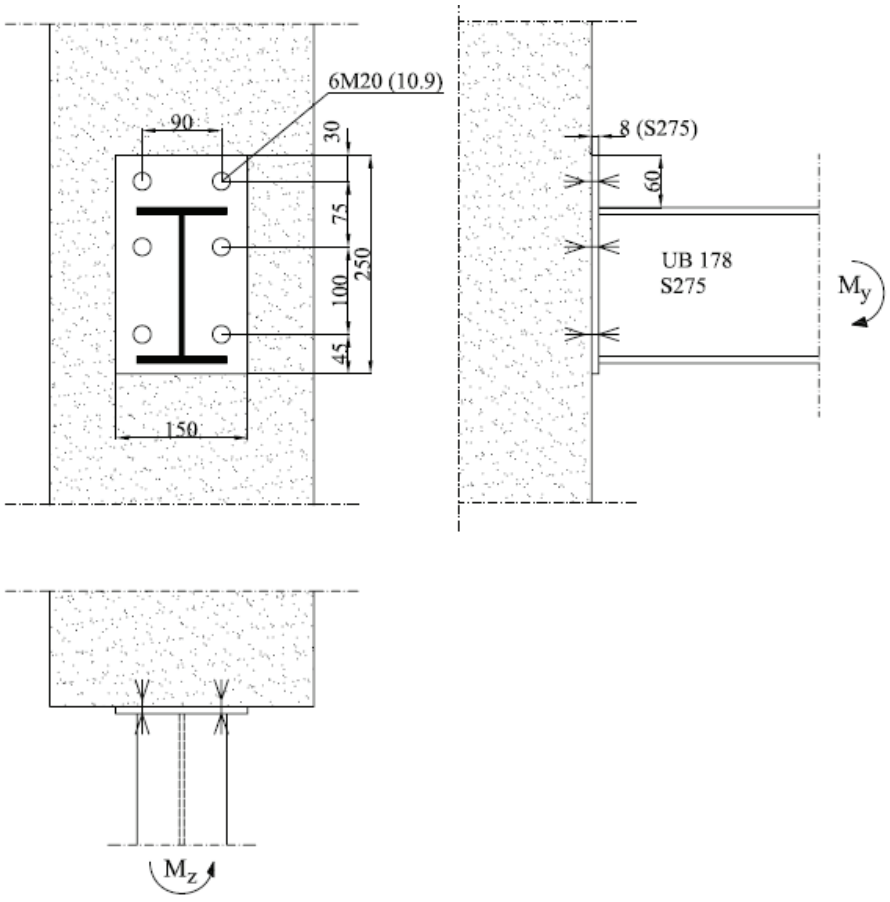

Figure 2.7 The geometry and loading of the modelled connection

In this study, no welds were modelled. The bolts were modelled as springs with equivalent stiffness with the bolts in the test. The bolts were considered to have washers of 4 mm thick underneath the nuts. With the nut height of 14 mm this gives for calculations the elongation length L_b of 44 mm, see figure 2.8 for meaning of the elongation length of the bolt.

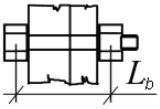

Figure 2.8 Elongation length of the bolt (EN 1993-1-8 2005)

2.3. Moment, Strong Direction

The moment resistance calculation for the strong direction-case is a straightforward application of the rules presented in the EN 1993-1-8 (2005). The procedure is presented next.

2.3.1. Tension Component Resistances

The tension components consist of bolts in tension, endplate bending and beam web tension. The resistances of the components are given in EN 1993-1-8 (2005) table 3.4. See figure 2.9 for a schematic presentation of the components present in this case. In real cases, the resistance of the welds on the tension side of the connection should also be checked.

Figure 2.9 The tension components: bolt tension, endplate bending, beam web tension (EN 1993-1-8 2005)

Following the rules presented in EN-1993-1-8 (2005), the deformations of the tensile bolts and the endplate bending should be taken into account, while the deformations of the welds and beam web can be omitted.

Bolt Tension

The bolt resistance is given by equation 2.1; the values for different variables in case considered are given in parentheses after the definition

$$F_{t.Rd} = \frac{k_2 f_{ub} A_s}{\gamma_{M2}} \tag{2.1}$$

where

$F_{t.Rd}$ = design tension resistance for one bolt,

k_2 = factor taking into account the type of the bolt (0.9)

f_{ub} = ultimate strenght of the bolt (1000 MPa),

A_s = tensile stress area of the bolt (245 mm^2),

γ_{M2} = partial safety factor for bolts (1.0[1]).

The bolt tension resistance per one bolt defined by equation 2.1:

$$F_{t.Rd} = \underline{176.4 \text{ kN}}$$

Endplate Bending

Endplate resistance has to be checked for individual bolt row required to resist tension and each individual group of bolt rows required to resist tension. In this case prying forces can be assumed to be present, as mentioned in the standard (EN 1993-1-8, table 6.2, note 2), so two T-stub failure modes must be checked, see fig 2.2. The third possible failure mode is the yield of the bolts only.

Bolt Row 1

The bolt row in the extended part of the endplate is considered with individual t-stub, see figure 2.10.

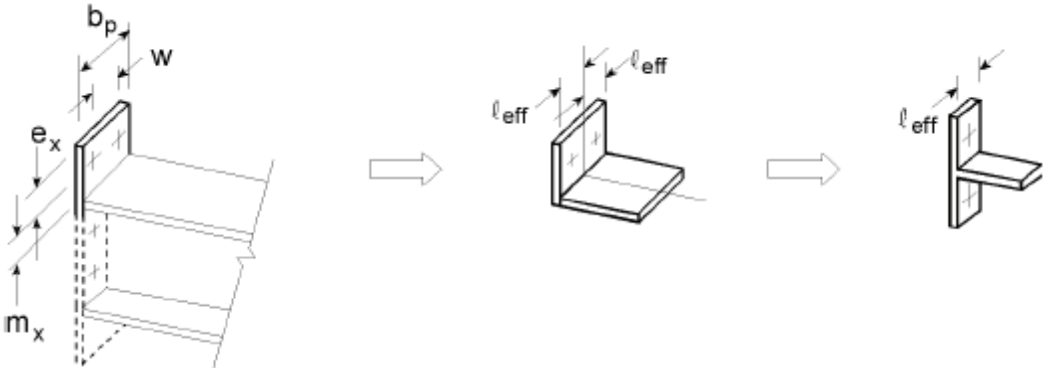

Figure 2.10 The modelling of extended part of endplate (figure from EN 1993--8 2005)

The resistance of the extended part of the endplate is given by finding the smallest effective length of the equivalent T-stub from equations 2.2-2.9. The meaning of vari-

[1] Safety factor of 1.0 is selected here because the aim of the calculation is to compare to the results of the FEM-analysis. In normal design and ambient temperature this factor is 1.25 according to EN 1993-1-8 (2005)

ables m_x, w, b_p and e_x are presented in figure 2.10 For this case they have values (note that no welds are included when the value of m_x is determined):

e_x = 30 mm (also e),
m_x = 30 mm,
w = 90 mm,
b_p = *150 mm.*

The effective length of t-stub for extended part of endplate is determined by first finding values of $l_{eff.cp}$ for circular yield mechanisms and $l_{eff.nc}$ for noncircular yield mechanisms of the endplate from the following equations (2.2 and 2.3):

$$l_{eff.cp} = \min \begin{cases} 2\pi m_x = 188.5 \text{ mm} \\ \pi m_x + w = 184.2 \text{ mm} \\ \pi m_x + 2e_x = \underline{154.2} \text{ mm} \end{cases} \tag{2.2}$$

$$l_{eff.nc} = \min \begin{cases} 4m_x + 1.25e_x = 157.5 \text{ mm} \\ e + 2m_x + 0.625e_x = 108.8 \text{ mm} \\ 0.5b_p = \underline{75 \text{ mm}} \\ 0.5w + 2m_x + 0.625e_x = 123.8 \text{ mm} \end{cases} \tag{2.3}$$

The effective lengths of T-stub for different failure modes are then given by equation (2.4) for mode 1 and equation (2.5) for mode 2:

$$l_{eff.1} = l_{eff.nc} \text{ but } l_{eff.1} \le l_{eff.cp} \quad \rightarrow l_{eff.1} = 75 \text{ mm} \tag{2.4}$$

$$l_{eff.2} = l_{eff.nc} \quad \rightarrow l_{eff.2} = 75 \text{ mm} \tag{2.5}$$

Now the calculated values for $l_{eff.n}$ can be used to find the moment resistance for both modes using equation 2.6:

$$M_{pl.i.Rd} = \frac{0{,}25 l_{eff.i} t_p{}^2 f_y}{\gamma_{M0}}, \tag{2.6}$$

where

$M_{pl.i.Rd}$ = plastic moment resistance of the failure mode *i*,
$l_{eff.i}$ = effective length of T-stub for *i*:th failure mode,
t_p = thickness off the endplate (8 mm),
f_y = yield limit of the endplate (275 Mpa),

γ_{M0} = material safety factor for endplate (1.0).

The plastic moment resistances from equation 2.6:

$M_{pl.1.Rd} = 330000$ Nmm
$M_{pl.2.Rd} = 330000$ Nmm

The plastic moment resistances $M_{pl.1.Rd}$ of the T-stub can be then used to find the tension resistances $F_{t.1.Rd}$ from equation 2.7:

$$F_{t.1.Rd} = \frac{4M_{pl.1.Rd}}{m_x}, \tag{2.7}$$

For failure mode 2 the tension resistance $F_{t.2.Rd}$ is found from equation 2.8:

$$F_{t.2.Rd} = \frac{2M_{pl.2.Rd} + n\sum F_{t.Rd}}{m_x + n}, \tag{2.8}$$

where
$n = e_{\min} = 30 \le 1.25m_x$

From equations 2.7 and 2.8:

$F_{t.1.Rd} = \underline{44 \text{ kN}}$,
$F_{t.2.Rd} = \underline{187.4 \text{ kN}}$.

The resistance of failure mechanism 3 is given simply by the sum of bolt resistances on the row 1, equation 2.9:

$$F_{t.3.Rd} = \sum F_{.t.Rd} \tag{2.9}$$

From equation 2.9:

$F_{t.3.Rd} = \underline{352.8 \text{ kN}}$.

The design tension resistance for bolt row 1 is 44 kN, from failure mode 1.

Bolt Row 2

For endplate between beam flanges, the resistance check is presented next. Between the flanges the check has to be done to both rows individually, and also as both rows grouped. First row 2 is considered individually. The meaning of variables m, m_2, m_3, e and p for bolt rows between the flanges are presented in figure 2.11:

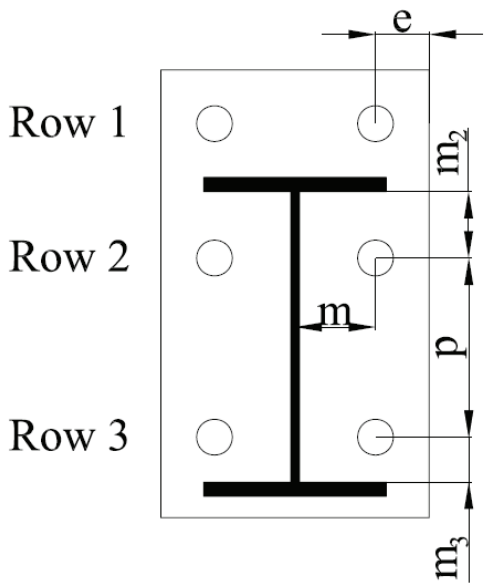

Figure 2.11 The variables for bolts between flanges

For this case the values for variables presented in figure 2.11 are:

$m = 42.6$ mm,
$m_2 = 37.1$ mm,
$m_3 = 25$ mm,
$e = 30$,
$p = 100$ mm.

The factor α is defined by first determining the two variables λ_1 and λ_2, see fig 2.12.

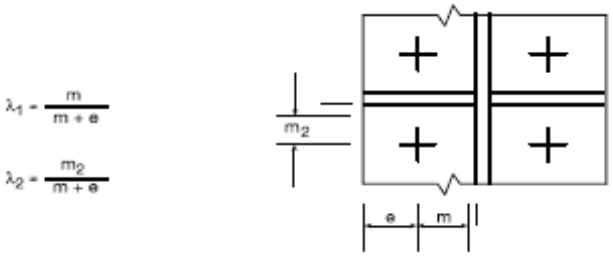

Figure 2.12 λ_1 and λ_2 (figure from EN 1993-1-8 2005)

For this case the values for λ_1 and λ_2 are

$\lambda_1 = 0.59$,
$\lambda_2 = 0.51$.

With these values the value of α is found from figure 6.11 from reference EN 1993-1-8 (2005), page 88:

$\alpha = 5.3$

The effective lengths of T-stub for individual bolts on row 2 are determined by first finding values of $l_{eff.cp}$ for circular yield mechanism and $l_{eff.nc}$ for noncircular yield mechanism from the following equations (2.10 and 2.11):

$$l_{eff.cp} = 2\pi m = 267.7 \text{ mm} \quad (2.10)$$

$$l_{eff.nc} = \alpha m = 225.8 \text{ mm} \quad (2.11)$$

After calculating equations (2.10, 2.11) the effective lengths for modes 1 and 2 are then defined by equations (2.4, 2.5):

$l_{eff.1} = 225.8$ mm
$l_{eff.2} = 225.8$ mm

The plastic moment resistance of the individual bolts on row 2 can now be calculated using equations (2.6-2.8), which gives the tension resistance for row 2, individual bolts:

$M_{pl.1.Rd} = 993520$ Nmm $\rightarrow F_{t.1.Rd} = \underline{93.29 \text{ kN}}$
$M_{pl.2.Rd} = 993520$ Nmm $\rightarrow F_{t.2.Rd} = \underline{275.52 \text{ kN}}$

For grouped bolts the effective length of T-stubs components $l_{eff.2}$ and $l_{eff.1}$ for $\sum l_{eff.1}$ and $\sum l_{eff.2}$ on second bolt row are found by similar procedure as for ungrouped bolts, equations (2.12, 2.13):

$$l_{eff.cp} = \pi m + p = 233.8 \text{ mm} \quad (2.12)$$

$$l_{eff.nc} = 0,5p + \alpha m - (2m + 0,625e) = 171.83 \text{ mm} \quad (2.13)$$

Bolt Row 3

For this case, the values for λ_1 and λ_2 are calculated as in row 2, but now using m_3 instead of m_2:

$\lambda_1 = 0.59$,
$\lambda_2 = 0.34$.

These give:

$\alpha = 5.8$

The effective lengths of T-stub for individual bolts on row 3 are determined by first finding values of $l_{eff.cp}$ for circular yield line and $l_{eff.nc}$ for noncircular yield line from the following equations (2.14, 2.15):

$$l_{eff.cp} = 2\pi m = 267.7 \text{ mm} \quad (2.14)$$

$$l_{eff.nc} = \alpha m = \underline{246.1 \text{ mm}} \quad (2.15)$$

The equivalent T-stub lengths can be then found from equations (2.5, 2.6):

$l_{eff.1} = 246.1$ mm
$l_{eff.2} = 246.1$ mm

The plastic moment resistance of the individual bolts on row 3 can now be calculated using equations (2.6-2.8), which gives the tension resistance for row 3, individual bolts:

$M_{pl.1.Rd} = 1082840$ Nmm $\rightarrow F_{t.1.Rd} = \underline{101.68 \text{ kN}}$
$M_{pl.2.Rd} = 1082820$ Nmm $\rightarrow F_{t.2.Rd} = \underline{257.22 \text{ kN}}$

For grouped bolts the effective length of T-stubs the components $l_{eff.cp}$ and $l_{eff.nc}$ for $\sum l_{eff.1}$ and $\sum l_{eff.2}$ for the third bolt row are found by equations (2.12, 2.13):

$l_{eff.cp} = 238.8$ mm,
$l_{eff.nc} = 194$ mm.

Bolt Rows 2 and 3 Grouped

For grouped rows 2 and 3, the length of equivalent T-stub is calculated as a sum from the lengths calculated from both cases, equations (2.14, 2.15, 2.16, and 2.17). The effective length for grouped modes are given by equations 2.18 and 2.19

$$\sum l_{eff.1} = \sum l_{eff.nc} \text{ , but } \sum l_{eff.1} \le \sum l_{eff.cp} \quad \rightarrow \sum l_{eff.1} = 365.8 \text{ mm} \tag{2.18}$$

$$\sum l_{eff.2} = \sum l_{eff.nc} \quad \rightarrow \sum l_{eff.2} = 365.8 \text{ mm} \tag{2.19}$$

After acquiring the T-stub lengths, the calculation proceeds by using the equations (2.7-2.9) to find first the plastic yield moments of the failure modes, and then tension resistance of the grouped bolt rows:

$M_{pl.1.Rd} = 1614800 \text{ Nmm} \rightarrow F_{t.1.Rd} = \underline{150.5 \text{ kN}}$,
$M_{pl.2.Rd} = 1614800 \text{ Nmm} \rightarrow F_{t.2.Rd} = \underline{167.1 \text{ kN}}$.

Beam Web Tension

The beam web tension resistance $F_{t.wb.Rd}$ is calculated by selecting the effective width of the web according to the effective T-stub lengths for each row, both individually and grouped, calculated earlier. The equation for beam web tension resistance is

$$F_{t.wb.Rd} = \frac{b_{eff,t,wb} t_{wb} f_{y,wb}}{\gamma_{M0}} \tag{2.20}$$

where:
$b_{eff,t,wb}$ = effective width of the web in tension (varies between rows)
t_{wb} = thickness of the web (4.9 mm),
$f_{y,wb}$ = yield limit of the web (275 Mpa).

Equation 2.20 gives for beam web tension resistances:

$F_{t.wb.Rd} = \underline{304.27 \text{ kN}}$ for row 2,
$F_{t.wb.Rd} = \underline{280.1 \text{ kN}}$ for row 3,
$F_{t.wb.Rd} = 492.9 \text{ kN}$ for rows 2 and 3 grouped.

For row 3 the resistance of rows 2 and 3 grouped deducted by the individual resistance of row 2 must be checked. This gives 492.9 – 93.29 = 399.6 kN > 280.1 kN and the individual resistance of row 3 is limiting.

2.3.2. Compression Component Resistance

The only compression component in this case is the compression of the beam lower flange, as the column is considered rigid, see fig 2.13.

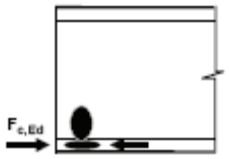

Figure 2.13 Schematic picture of beam flange compression (EN 1993-1-8 2005)

Beam Flange Compression

The beam flange compression resistance can be found by using equation 2.21:

$$F_{c,Rd} = \frac{M_{c,Rd}}{h - t_{fb}} \tag{2.21}$$

where:

$F_{c,Rd}$ = the beam flange compression resistance,

$M_{c,Rd}$ = the beam plastic moment resistance ($W_{pl} f_y$)

W_{pl} = plastic bending resistance of the beam (171 cm^3)

f_y = yield limit of the beam (275 Mpa),

h = height of the beam (178 mm),

t_{fb} = beam flange thickness (7.9 mm).

Equation 2.21 gives for compression resistance:

$F_{c,Rd} = \underline{276.5 \text{ kN}}$

2.3.3. Summary of the Components

The components for different rows are summarized in tables 2.1 – 2.3. It must be noted that because the grouped tension resistance from row 2 and 3 is smaller than the sum of individual resistances of the rows, the rows have to be treated as grouped. According to the rules given in reference EN 1993-1-8 (2005), the row further away from the compression center (row 2) gets its individual resistance (93.3 kN), and row 3 takes on the

grouped resistance deducted by the resistance of row 2 (150.5 – 93.29 = 57.12 kN). The location of the compression center has to be considered individually for moments acting in other directions.

Table 2.1 Tension components on bolt row 1

component	Resistance (kN)
Endplate bending	***44.0***
Bolt tension	352.8

Table 2.2 Tension components on bolt row 2

component	Resistance (kN)
Endplate bending	***93.3***
Beam web in tension	304.2
Bolt tension	352.8

Table 2.3 Tension components on bolt row 3

component	Resistance (kN)
Endplate bending	***57.1***
Beam web in tension	280
Bolt tension	352.8

For this case, the tension side is critical, as the sum of tension component resistances (194.5 kN) is smaller than the compression resistance (276.5 kN).

2.3.4. Moment Resistance of the Joint

The moment resistance is calculated from equation (2.22):

$$M_{j,Rd} = \sum_r h_r F_{tr,Rd} \,, \tag{2.22}$$

where

$M_{j,Rd}$ = the joint design moment resistance,

h_r = the distance of the bolt-row from the center of compression,

$F_{tr,Rd}$ =the effective design tension resistance of bolt row r.

The values of design resistances are defined in section 2.3.3. The values for $h_1 – h_3$ can be found from the geometry, when the compression center is assumed to be at the middle of the lower flange:

$h_1 = 0.204$ m,

$h_2 = 0.129$ m ,

$h_3 = 0.029$ m .

Equation 2.22 gives for moment resistance of the joint:

$$M_{j,Rd} = (0.204 * 44 + 0.129 * 93.29 + 0.029 * 57.21) \text{ kNm} = \underline{\underline{22.7 \text{ kNm}}}$$

This is the moment resistance of the joint in Fig 2.7, For the positive strong axis moment $M_{y,}$ following the rules presented in EN 1993-1-8 (2005).

2.4. Moment, weak direction

For the weak direction moment, the Eurocode (EN 1993-1-8 2005) does not give suitable components. In reference (Heinisuo, Laine, Lehtimäki 2009) a proposal is made for potential tension and compression components. These components, and the components assumed to be active in this case, are presented in fig 2.14 :

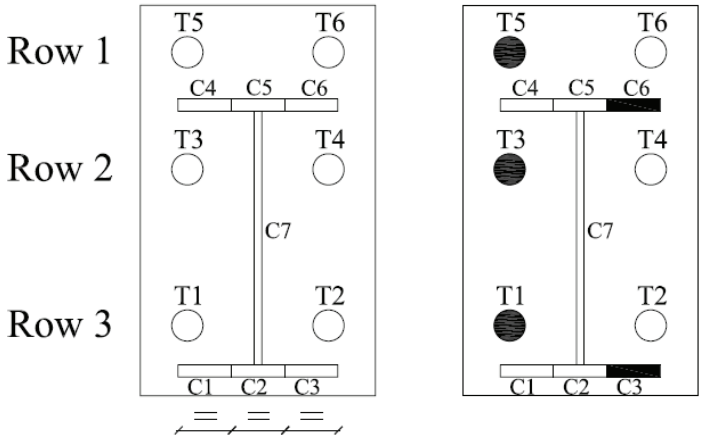

Figure 2.14 All potential components according Heinisuo, Laine, Lehtimäki (2009), and assumed active components acting in the weak axis bending case studied (right).

One third of the flange is considered active on the compression side. With the moment directed to right side of figure 2.14, the active tension components are T5, T3 and T1. The active compression components are C3 and C6. The rotation axis is supposed to be a line passing through the midpoints of compression components C3 and C6.

2.4.1. Tension component resistance

The previously calculated value for the bolt tension resistance applies to this case also. For the endplate bending, it is supposed that the yield lines given in the standard EN1993-1-8 (CEN 2005b) do apply, but have to be considered again for this direction to find the most critical one for this case.

Endplate Bending

Endplate resistance calculations change from the strong direction case discussed earlier. The measures and nomenclature for weak direction calculations are as in section 2.3 in corresponding locations. The bolts in the extended part of endplate have to be considered both as individuals and as a group, depending whether both bolts are in tension or not. For the bolts between the flanges, the yield mechanisms are supposed to be the same as for the strong direction case.

Bolt Row 1

In this case, the compression center is assumed to be located so that the tension component T6 is not active, and therefore the check has to be done as bolts as individuals only, see figure 2.2. Note that the equations in figure 2.2 are for two bolts, and only one is active in this case. The effective lengths for different yield mechanisms are now given by equations (2.23) and (2.24)

$$l_{eff.cp} = \min \begin{cases} 2\pi m_x = 188.5 \text{ mm} \\ \pi m_x + 2e_x = \underline{154.2} \text{ mm} \end{cases} \tag{2.23}$$

$$l_{eff.nc} = \min \begin{cases} 4m_x + 1.25e_x = 157.5 \text{ mm} \\ e + 2m_x + 0.625e_x = \underline{108.8 \text{ mm}} \end{cases} \tag{2.24}$$

After calculating equations (2.23, 2.24) the effective lengths for modes 1 and 2 are then defined by equations (2.4, 2.5) again:

$l_{eff.1} = 108.8$ mm

$l_{eff.2} = 108.8$ mm

The plastic moment resistance for T-stub on row 1 can now be calculated using equations (2.7 and 2,8),

$M_{pl.1.Rd} = 478720$ Nmm

$M_{pl.2.Rd} = 478720$ Nmm

Now the tension resistance for failure modes 1 and 2 can be calculated by equations (2.8, 2.9).

$F_{t1,Rd} = \underline{63.8\ kN}$

$F_{t1,Rd} = \underline{158.2\ kN}$

The values for tension resistance are now for two bolts, so the limiting value is reached by dividing the result by two:

$F_{t1,Rd} = \underline{32.0\ kN}$

Bolt Rows 2 and 3 Grouped

It is clear from the section 2.3.3, that the bolts between the flanges act as group. The reference CEN (2005) does not give guidelines on how to divide the grouped resistance in this case, as both bolts are equally distanced from the compression center. In this study the grouped tension resistance is divided equally between the two rows. This is also divided by two, because only one bolt per row is active.

$F_{t2,Rd} = \underline{37.6\ kN}$
$F_{t1,Rd} = \underline{37.6\ kN}$

2.4.2. Compression Component Resistance

The compression component is considered to be one third of the beam flange according to the reference (Heinisuo, Laine, Lehtimäki 2009). The resistance of compression components C3 and C6 are calculated simply as the compression resistance of the piece (eq. 2.24), as web is not active:

$$F_{c,Rd} = A_f f_y \tag{2.24}$$

where

$F_{c,Rd}$ =compression resistance of the flange,

A_f = the area of the flange compressed ($101.2 / 3 * 7.9 = 266.5\ \text{mm}^2$),

f_y = yield limit of the flange (275 Mpa).

Equation 2.24 gives for compression resistance per one flange:

$F_{c,Rd} = \underline{73.29\ \text{kN}}$

Here should be noted that the flange compression is assumed to be the same for both flanges. As the case is not symmetric for both axes, this assumption is probably unrealistic.

2.4.3. Summary of the Components

For this case only the critical component resistances are presented, see table 2.4:

Table 2.4 The limiting components for weak axis case

row	Component	$F_{Rd}/bolt$
Tension 1	Endplate bending	***32.0***
Tension 2	Endplate bending	***37.6***
Tension 3	Endplate bending	***37.6***
compression	Flange compression	***73.2***

From table 2.4 it can be observed that the sum of the tension components (32+ 37.6+ 37.6 = 107.2 kN) is smaller than the resistance of the compression side (2*73.2 = 146.4 kN) and for this case the compression side is not critical.

2.4.4. Moment Resistance of the Joint

The moment resistance is calculated from equation (2.22):

$$M_{j,Rd} = \sum_r h_r F_{tr,Rd} ,$$

where

$M_{j,Rd}$ = the joint design moment resistance

h_r = the distance of the bolt-row from the center of compression,

$F_{tr,Rd}$ =the effective design tension resistance of bolt row r.

The values of the design resistances are defined in section 2.4.3. The values for $h_1 – h_3$ are for this case approximately 0.079 m for all of the rows.

Equation 2.22 gives for moment resistance of the joint:

$M_{j.Rd}$ = 0.079*(37.6+37.6+32) kNm= 8.5 kNm

This value is the moment resistance of the joint presented in figure 2.7,
for weak axis bending moment M_z.

3. MODELLING OF THE JOINT BY SAFIR

3.1. SAFIR

SAFIR is a software for evaluating structures in ambient conditions and subjected to fire. The program is developed at the University of Liege. SAFIR is based on the finite element method (FEM) and can be used to study one, two, and three-dimensional structures. The different elements present in SAFIR are 2D solid elements, 3D solid elements, beam elements, truss elements and shell elements.

3.1.1. Overview of the Analysis Procedure

In SAFIR, the temperatures for different structures are defined first, and the resulting output files are connected to structural model input files. Then a series of static or dynamic analyses are done with the varying temperatures. The input files can be made with a text editor or some third party graphical preprocessor software. GiD is a widely used program for preprocessing, and required problem type files for SAFIR are included with SAFIR. The SAFIRWIZARD -program is also included in SAFIR, suitable for creating input files for hot rolled H-sections. In figure 3.1 a schematic presentation of the analysis is presented.

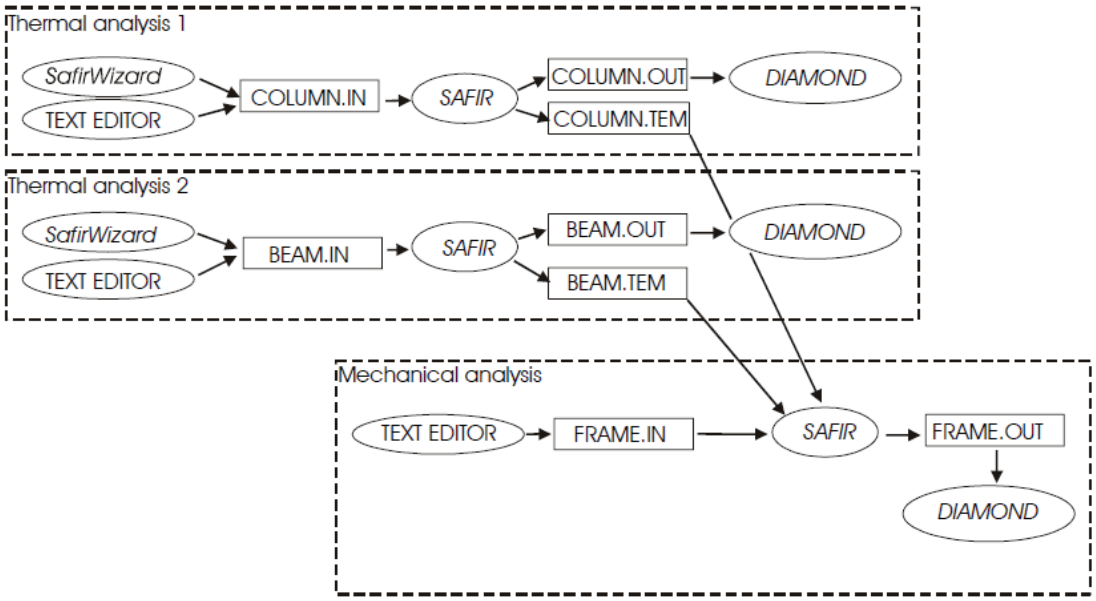

Figure 3.1 Schematic presentation of analysis procedure in SAFIR (Franssen 2007)

Output files can be analyzed either with third party graphical postprocessors or with Diamond included with SAFIR. An extractor for creating Excel spreadsheets from the output files is also included with SAFIR. (Franssen 2007). A detailed description of the structure of all the input and output files can be found in the SAFIR user manual (Franssen 2007).

3.1.2. Thermal Analysis

The temperature calculations are transient and based on Fourier equations. Temperatures of both 2D and 3D objects can be analyzed. SAFIR has some predefined materials and the user can introduce maximum of 5 own materials per calculation, either with constant or temperature dependant properties (Franssen 2007). Voids can be taken into account in 2D solid calculations. The result files of a temperature analysis are labelled OUT and TEM or TSH-files. The OUT file is meant for post processing and .TEM and .TSH files to be used in the structural analysis. The temperature distribution file .TEM for beam elements is calculated only in the plane of the cross section, and thus the temperature is uniform along the length of the element. The temperature file .TSH for shell elements is calculated along the thickness of the shell, and no heat is transferred along the length of the shell. The temperature distribution can vary from element to element, making modeling of e.g. varying fire exposure possible. A detailed description of the thermal calculations is presented in the paper Elements of theory for SAFIR 2002 (Franssen, Kodur, Mason 2007).

3.1.3. Structural Analysis

After calculating the different temperatures for beam and shell elements, the resulting output files can be referred to in the input file for structural analysis. Structural calculations can be done in either 2D or 3D. In 2D calculations beam and truss elements are present. In 3D calculations beam, truss and shell elements are present. For 3D solid elements material model is yet to be validated and they are not available (Franssen 2007). No semi rigid connections are possible, only totally fixed or totally free. Joints can be made by determining two nodes at the same location to have a slave-master relationship. Details of the structural calculations are presented in (Franssen, Kodur, Mason 2007). In this study a dynamic analysis with modified Newton-Raphson procedure for convergence with “no comeback” was used. “No comeback” means that the simulation is stopped the first time the left term equation $Kq + C\dot{q} + M\ddot{q} = F$ is not positive (Franssen 2007)[2]. If comeback is chosen, each time the term is negative or the number of iterations required to obtain convergence is greater than 3, the time is reset at last converged point and the simulation restarts with smaller time step. This goes on until time step is smaller than parameter TIMESTEPMIN. After three consequent iterations

[2] Note: this criteria presented in the documentation of SAFIR is for 1D-cases. For cases with more dimensions the criteria should be in matrix form.

where convergence is reached in less than three iterations, the time step is multiplied by factor of two (Franssen 2007).

3.2. General issues about Modelling with SAFIR

The study was started by the modeling of very simple models to learn about the program and its functionalities. The first phase was to find a suitable method to model the frictionless contact between the endplate and the column, because SAFIR has no prebuilt contact elements. The first models consisted of 400 mm long beam, endplate and very thick plate. The functionality of the contact solution was tested with this model. After getting experience from the simplified model half of the frame from Wang (2007) experiments was modelled. The preprocessor GID, supported by problem type files included with SAFIR, was used to model the geometry.

3.2.1. Elements used in modelling

Two element types were used in the models, truss and shell elements. The truss element is defined by its cross sectional area and material type, only one strain, temperature and material is present in each truss element. All integrations for truss elements are done analytically, and therefore no integration points are give for truss elements. The degrees of freedom for truss element are presented in figure 3.2. (Franssen et al 2002).

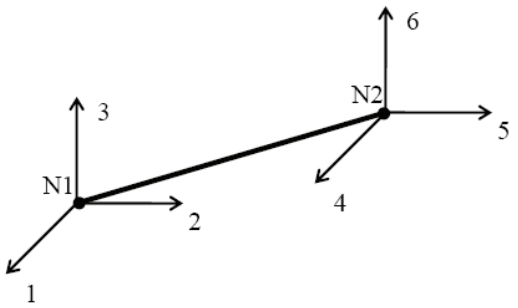

Figure 3.2 The degrees of freedom at nodes for truss element (Franssen et al 2002)

The shell element has four integration points on the surface of the element. The integration is done by the method of Gauss. The number of integration points along the thickness of the element is defined by user, from 2 to 10. The integration points of shell element are presented in figure 3.3. (Franssen et al 2002).

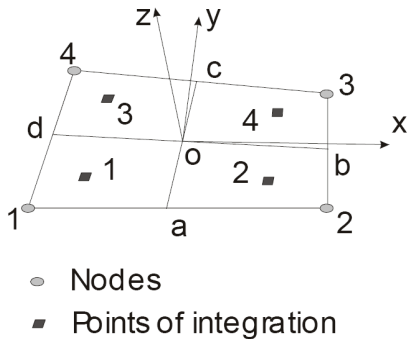

Figure 3.3 Geometry and local axis of shell element (Franssen et al 2002)

3.2.2. Contact Problem

SAFIR does not include contact elements, and finding a method to model these was the first step. The approach was to use truss elements with no tension resistance to model the contacts. The initial tests using very simple truss made of these elements, and calculated by hand also, demonstrated that the approach was working. The material used to model the contacts was concrete according to Eurocode, with the tensile strength set as zero.

Another problem that was found later on the modeling was connecting two nodes with restricted degrees of freedom with the contact trusses, resulting in access violation-errors in calculations. This was avoided by leaving the contacts out from the edge of the plates, where some boundary conditions had to be introduced. The contact trusses were connected to the endplate and column by creating extra nodes to the junction points of contacts and shell elements, and defining each node at the same location to have the same translational degrees of freedom with command SAMEALL in the FIXATIONS-group of input file.

3.2.3. Precision and Mesh Refinement

In SAFIR the input file user is required to decide a number of precision which is required for convergence to be achieved. This number is also used as small number in the calculations (Franssen 2007). The starting value for this is recommended as 0.0005 for dynamic calculations. A series of simulations were done to find the largest value of precision before the results scattered. The results of these simulations are plotted in figure 3.4. The rotations in figure 3.4 are calculated according to the displacements of the free end of the beam. The moment is the moment acting on the joint, calculated simply by multiplying the acting force by the length of the beam.

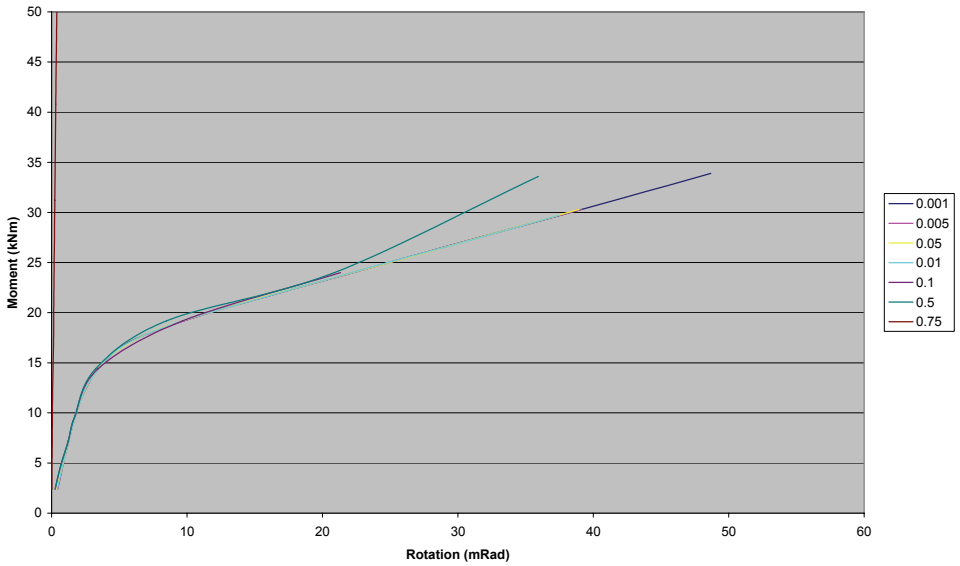

Figure 3.4 Comparison of different values of precision

It can be seen that precision starts to effect first time when it is of value 0.5. Value 0.05 was chosen for the precision in simulations as the calculation time is reduced with relaxed requirement of convergence.

Some simulations with a more refined mesh were also done, and it was found that doubling the refinement resulted in no significant change when considering the results, but in a great increase of the computation time. The moment-rotation curve comparison between different mesh refinements for simple model with positive moment M_y is in figure 3.5.

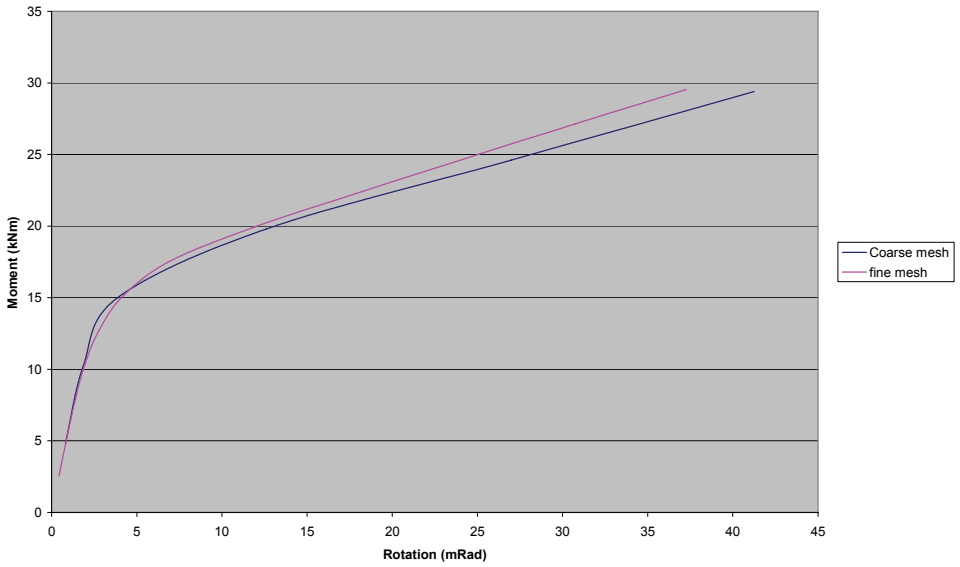

Figure 3.5 Comparison of result with different mesh refinement

It can be seen that the results do not vary much, and that the elastic phase of the curve is very similar for both meshes.

4. SIMPLE MODEL

4.1. Model Description

The first model was such that the column of the test was replaced with a thick plate, or rigid foundation. The contact between the endplate and the foundation was supposed to be frictionless. The potential contact area was modelled using the truss elements described in section 3.2.1. As the wanted result was the moment resistance of the joint, a point load was placed to the end of the beam. This load was then increased until the joint failed. The details of the model are presented in the next sections. An input file for strong direction moment is in Appendix 1.

4.1.1. Geometry and Mesh

The column section was ignored in the first model. Instead of the column, a very stiff foundation was present in the model. The foundation was made of the same material type as other shell components, and had a thickness of 100 mm. The foundation was created by copying the endplate with an offset to the z-direction, which was selected to be 5 mm. The contact elements and bolts were connecting the endplate and the foundation from each opposing node. Figure 4.1 illustrates the geometry and the mesh of the model.

The mesh was defined in GID as a structured mesh. The mesh at the endplate was created according to the mesh at the end of the beam, so that nodes coincided. This caused some changes in the element size in the endplate, as the structured mesh was created by setting the division on lines of the geometry. The element size on the endplate and foundation was approximately 1 cm x 1 cm. In the beam the element size was approximately 2 cm x 1 cm (b x h). The coordinate system of SAFIR is shown in figure 4.1.

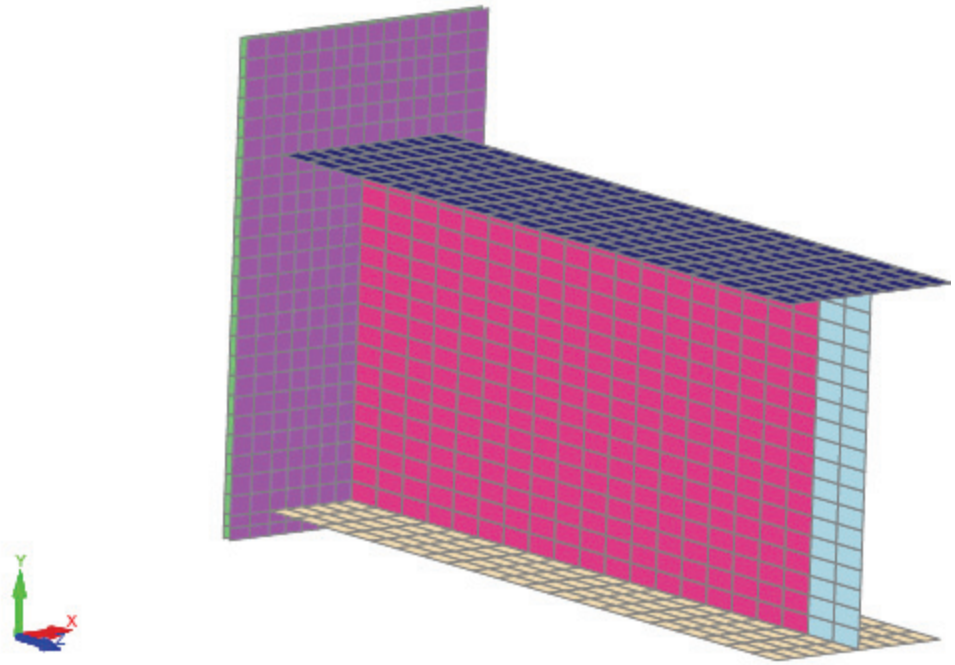

Figure 4.1 The coordinate system, geometry and mesh of the simple model

It should be noted that, due to the fitting of the mesh, the bolts are not exactly placed as in the joint in the test. The largest offsets from the test are 4.5 mm.

Because the whole way of modelling the bolts was approximate by nature, the error caused by the approximate location of the bolts was considered insignificant. The end of the web was made thick to avoid the local failure near the loading. No welds were modelled.

4.1.2. Elements

The mesh was done by using shell and truss elements. The contacts and the bolts were modelled using truss elements. The elastic modulus of bolts was not changed, and as the length of the bolt was chosen to be 5 mm when creating the geometry, the only variable was the cross section area. The cross section area of the trusses presenting bolts was defined by demanding the stiffness of the bolt and truss to be the same. The longitudinal stiffness of both the bolt and the truss element are set equal in equation 4.1:

$$\frac{L_1}{A_1 E} = \frac{L_2}{A_2 E} \tag{4.1}$$

where

L_1 = elongation length of the bolt (44 mm) (see section 2.2),

L_2 = length of the element (5 mm),

E= elastic modulus of steel (210 GPa for both cases),

A_1 = tension area of the bolt in experiment (245 mm^2),
A_2 = cross section area of the truss element in the model (mm^2)

The area of the truss can be solved from the equation (4.1):

$$A_2 = \frac{L_2}{L_1} A_1 \Rightarrow A_2 = 28 \text{ mm}^2$$

The cross section area of the contact truss elements was first defined as 1 cm^2, as the element size in the endplate and the foundation plate was approximately this. This approach was found to be functional and was kept in all the simulations. The large cross sectional area of the contact elements made them stiff, and resulted in a good representation of contact.

Shell elements of SAFIR were used to the model beam, the endplate and the foundation. Only the thickness of the elements had to be defined in the .TSH files, as this simulation was done in ambient temperature. The thickness of the elements is as in the experiment, except for the end of the beam where the thickness of the web was made ten times as large (49 mm) to prevent the local failure of the web under the point load. The roundings of the beam or welds at the endplate were not modelled.

4.1.3. Materials

SAFIR includes some predefined materials, and these were used in the modeling. All shell elements were made of material PLSTRVML, which is a simplified 2D plane stress bilinear model for steel (Franssen 2007). Material PLSTRVML was defined in the input file for SAFIR as follows:

```
PLSTRVML
210e+9   3.00e-01   2.75e+08 2.1e+9
```

Where the first value stands for elastic modulus E (Pa), the second value for Poisson's ratio v, the third for yield stress f_y (Pa) and the fourth for the slope of the strain-hardening branch of the curve (Pa). In figure 4.2 is the stress – strain curve used for steel in the simple model. The strain hardening modulus was selected, according to rules given in Eurocode (EN 1993-1-5 2006, Annex C), to be 1/100 of the elastic modulus.

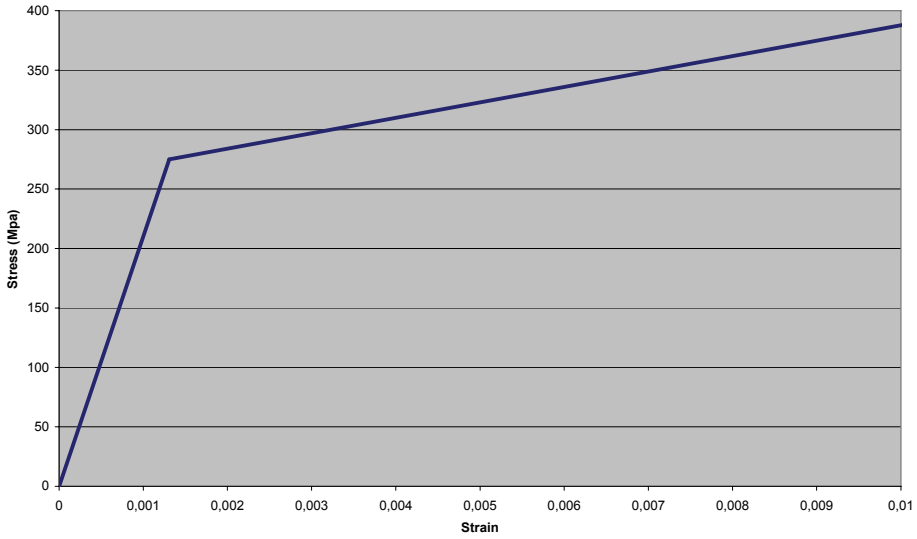

Figure 4.2 The stress – strain curve for material type PLSTRVML

The bolts were modelled with material BILIN, which is a bilinear uniaxial material valid at 20 °C (Franssen 2007). The bolt had a yield strength of 900 MPa, and otherwise same values as the shells. The stress strain curve for BILIN is presented in figure 4.3

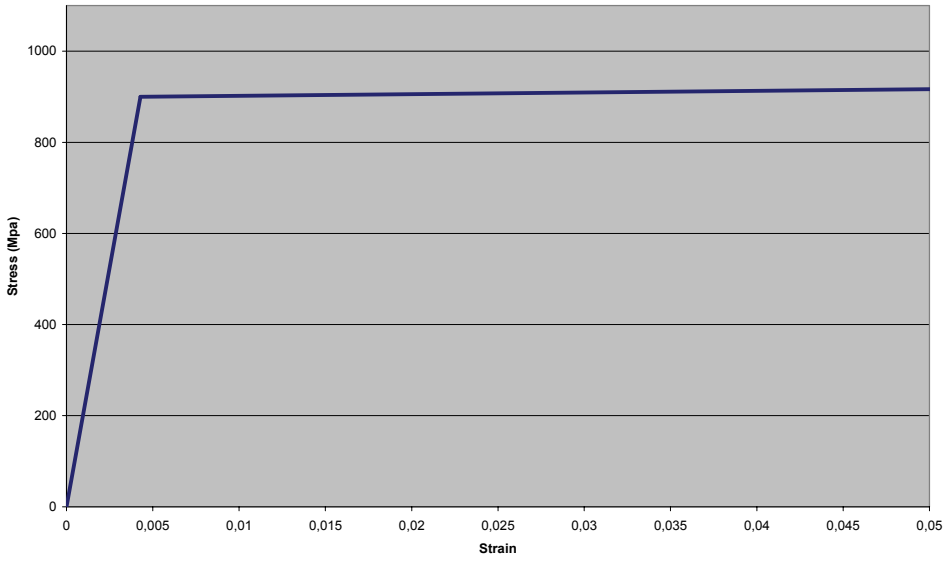

Figure 4.3 The stress- strain curve of material type BILIN

The contact elements were modelled using material SILCONC_EN, which is a concrete material according to EN 1991-1-2 (2005) (Franssen 2007) The other values are set as SAFIR defaults, but the tensile strength was set to zero to model the contact. The stress-strain curve following EN 1991-1-2 (2005) is plotted in figure 4.3.

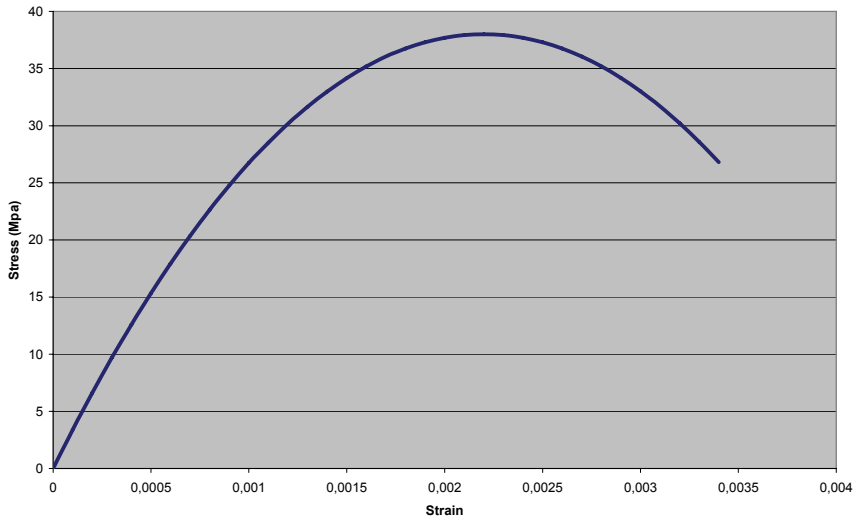

Figure 4.3 Stress-strain relationship of SILCONC_EN material

4.1.4. Boundary Conditions

The lower end of the endplate was supported in y-direction and vertical sides in x-direction to prevent the movement of a rigid body. In addition, the upper end of the endplate was constrained in z-direction, as the lack of contacts in the area caused convergence problems. In the test prying effect was occurring, and it was expected that the contact appears at the upper end of the endplate for strong direction moment. It was assumed that the prying effect was also present in the weak direction case in this study. The foundation was supported rigidly in all translation and rotation directions from the edges. Constraints are presented in figure 4.5.

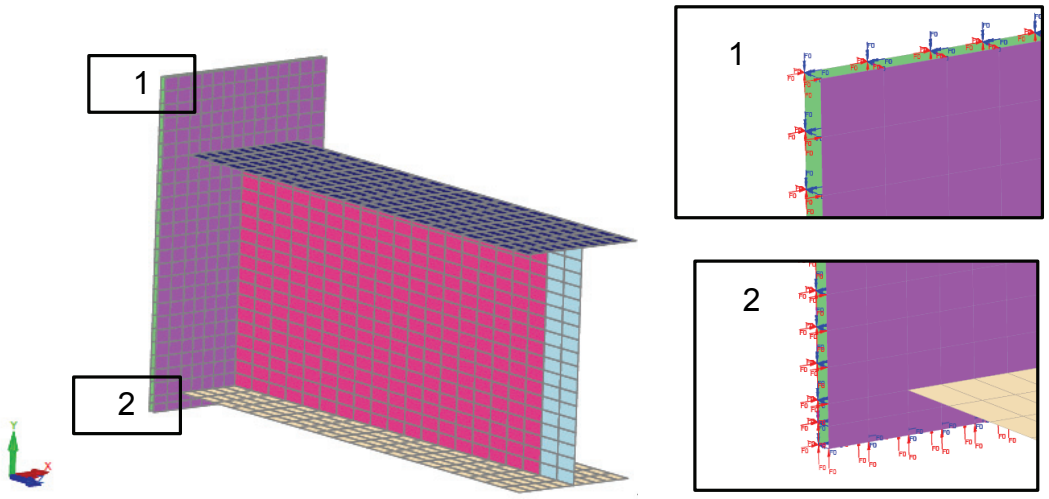

Figure 4.5 Boundary conditions of the simple model

4.1.5. Loading

The load was assigned as a point load at the end of the beam, either at the crossing of the upper flange and the web for strong axis case or at the middle of the web for weak axis case. The load function was of the type "F1PS", which multiplies the load vector by factor of one every second. The load vector magnitude was 2 kN for the strong axis case, and 1 kN for the weak axis case. Load vectors for the two cases, strong axis moment M_y and weak axis moment M_z, are presented in figure 4.6.

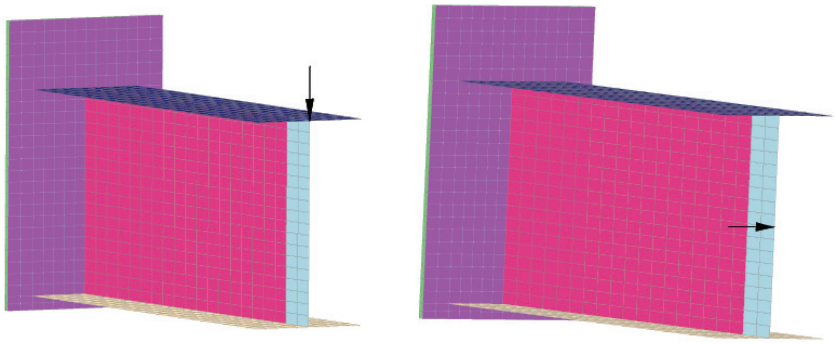

Figure 4.6 Load vector for M_y (left) an M_z (right)

4.2. Results

For both cases, the results are presented next. The moment-rotation curves, calculated according to the beam theory, using displacements from the end of the beam are given. The results are compared to the results of the calculations by the component method. To better understand the displacements in the endplate area, plots of displacements at the beam flange and web at the endplate are given with varying moment loads.

4.2.1. Positive Moment to the Strong Direction

The moment reached in the simulations was 60 kNm, while corresponding rotation was almost 200 mRad. This exceeds, almost three times, the result calculated by component method (22.7 kNm). See section 2.3.4 for the calculation of the moment resistance. The moment-rotation curve, moment resistance from component method and the elastic limit moment 2/3*$M_{j.Rd}$ are plotted in figure 4.7. It should be noted that infinite strains are allowed for steel materials.

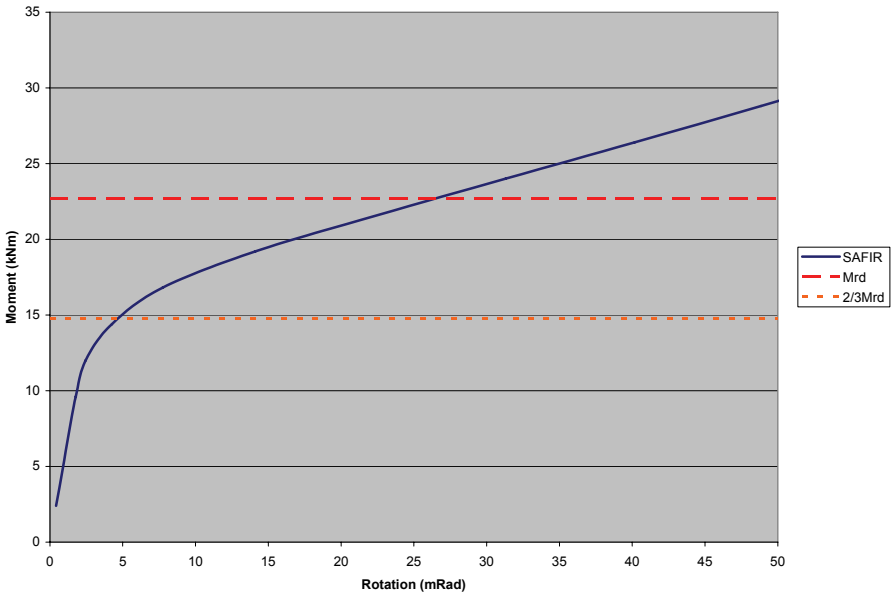

Figure 4.7 The moment rotation curve from the simulation

It is stated (Del Savio et al 2009) that the rotations over 50 mRad have no meaning in real structures, and are omitted from the data. The rotation of 35 mRad is considered a limit for suitable rotation in the earthquake design of joints in the standard (EN 1998-1 2005), so the rotations reached by simulation in SAFIR can be considered very large.

Visual observations can be made from the simulations too. The displacements are plotted at the nearest points to the different limit moments. 14.4 kNm for elastic limit moment, 21.6 kNm for moment resistance, and 60 kNm for the final failure in the simulation. The displacement visualization is presented in figure 4.8. The scale in this figure is 1.

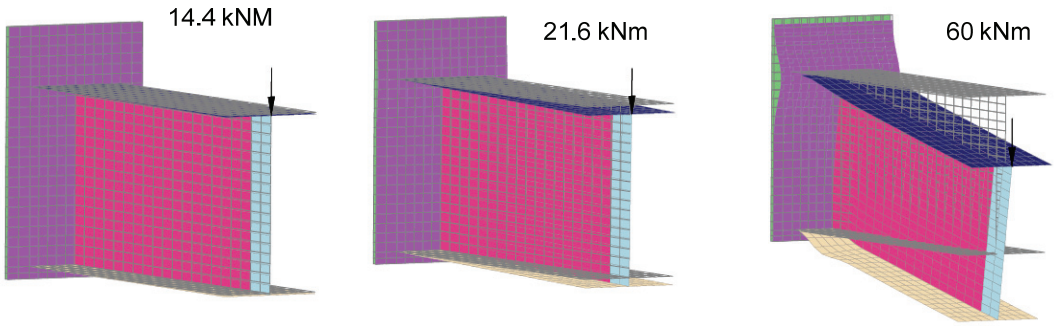

Figure 4.8 DIAMOND-visualization of the simulation with varying M_y . Scale 1.

It can be seen that the displacements are considerably unnoticeable at the elastic limit. When the moment increases to the value of the calculated resistance, the beam end deflection is clearly noticeable, but still subtle. In addition, some endplate bending around the upper flange can be seen. When the ultimate moment in the simulation is reached, the beam end displacement is very large, and endplate is clearly deformed. The beam lower flange has started to buckle, and the final collapse seems to be caused by

this loss of stability. For better detail of the deformations of the lower flange and endplate, see figure 4.9.

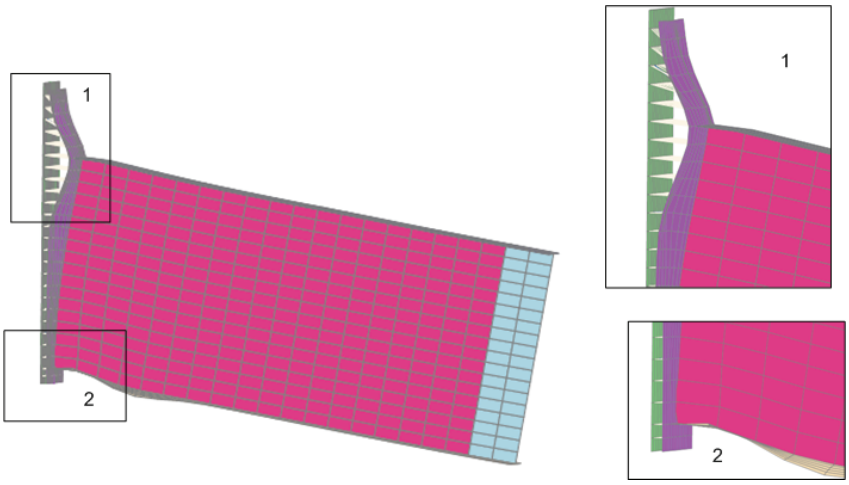

Figure 4.9 Side view and details at collapse, scale 1

A big deformation in the lower flange can be observed, and the negative displacement near the bottom of the beam web can be seen (detail 2). The endplate has bended significantly, and the upper edge of the plate has moved noticeably downwards. The beam end displacement is very large. For better view of the displacements at the junction of the endplate and the beam web, see figure 4.9.

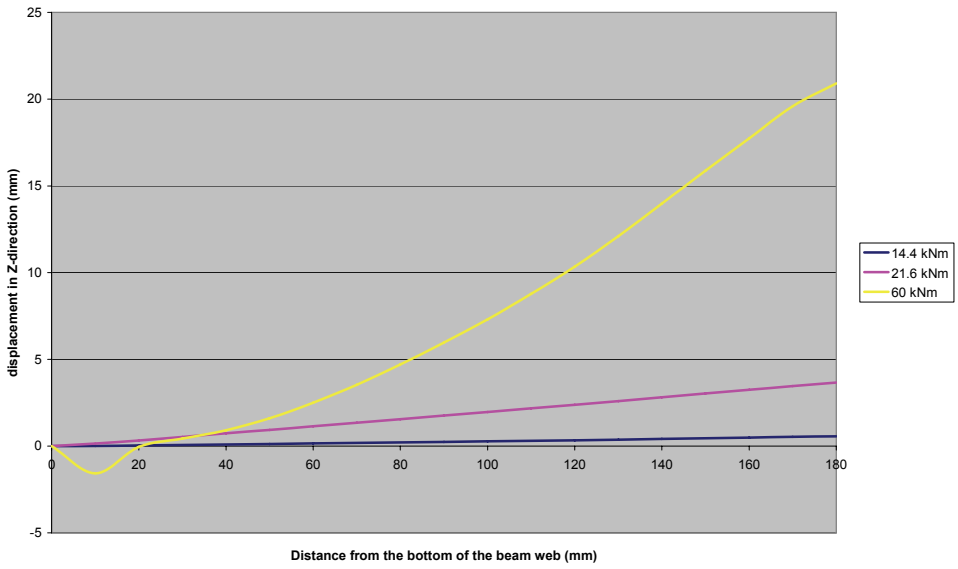

Figure 4.9 Beam web/endplate displacements

The displacements at the endplate are plotted so that the left end of the x-axis represents the node in lower flange, and the right end the upper flange. For the elastic limit and resistance moment, the displacements are linear from top to bottom. For the 60 kNm, there is a negative (to the z- direction) displacement at the second node of the flange. This indicates that the contacts have failed at that area.

4.2.2. Moment to the Weak Direction

The moment reached the maximum of 9.6 kNm in the simulation. This was 14% larger than the result reached with the component method, significantly less than the strong direction simulation was. The moment-rotation curve along with the moment resistance from the component method and the elastic limit moment $2/3*M_{jRd}$ are plotted in figure 4.10. It can be seen that the yield starts at approximately the same point with both the component calculation and the simulation.

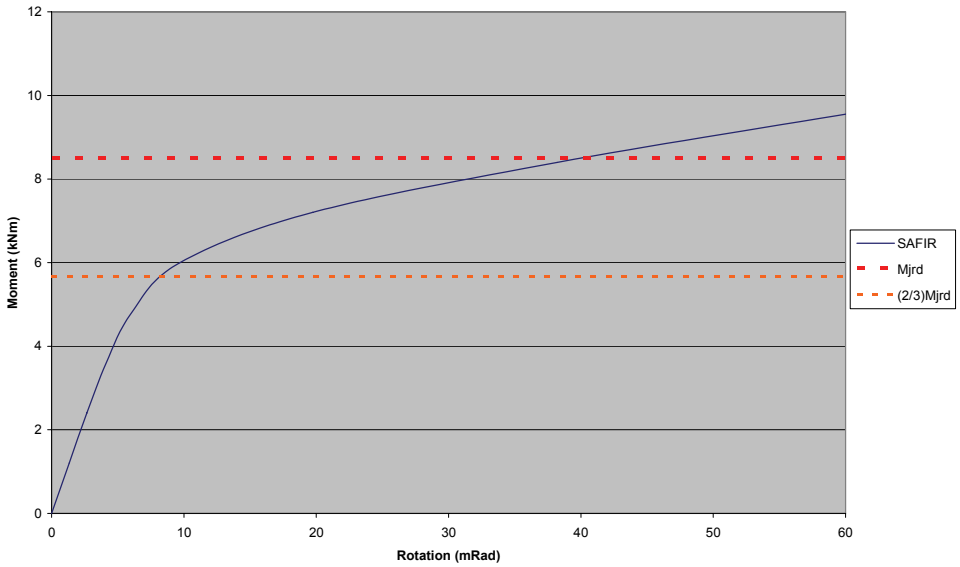

Figure 4.10 The moment-rotation curve from the simulation, M_z

In figure 4.11 there is a Diamond-visualization of the simulation near the calculated points of interest, elastic limit moment, moment resistance and the termination of the simulation. The scale in the figure is 2.

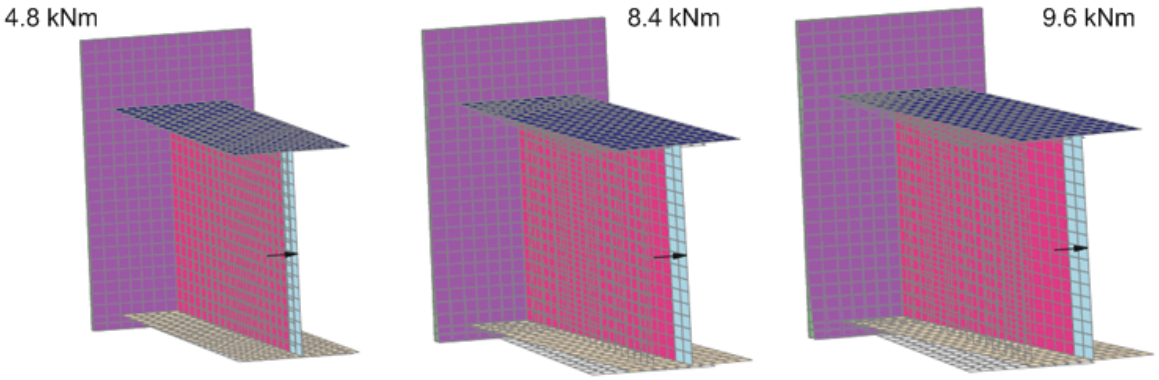

Figure 4.11 Diamond-visualization of the simulation, M_z, scale 2

It can be observed, that the displacements are subtle in this case, hard to notice even with the used scale. However, as the joint has now only symmetry relative to the Y-axis,

the bending causes displacement not only to the X-direction, but also some to the Y-direction. This results in larger displacements in the lower flange, as the beam end moves to the Y+ -direction. This can be better observed from the figures 4.12 – 4.14.

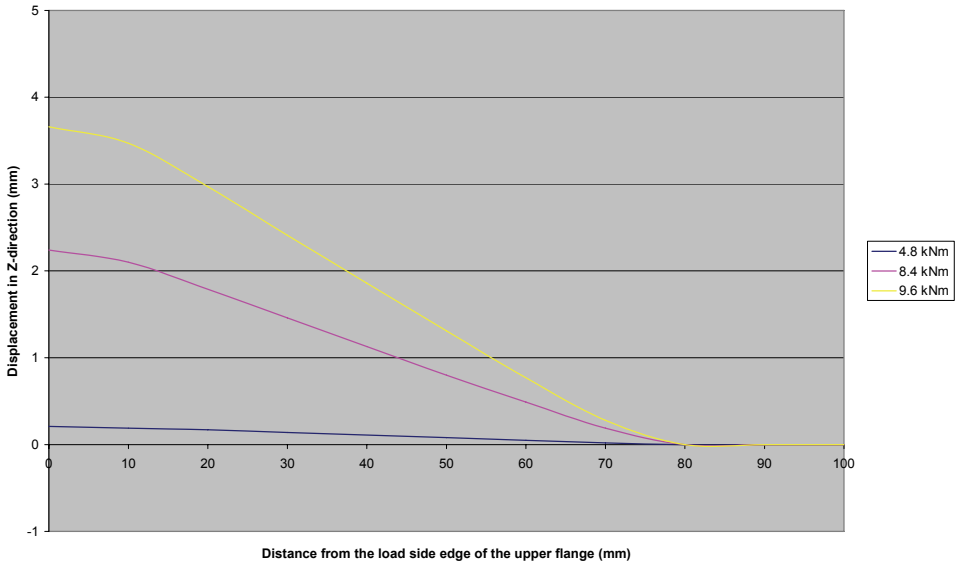

Figure 4.12 Upper flange/endplate displacements with varying moments, M_z

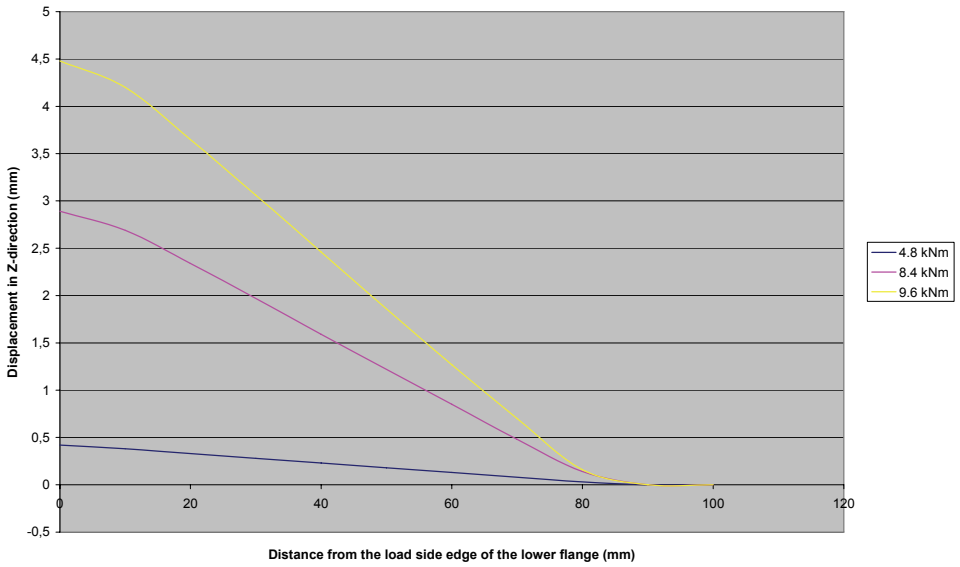

Figure 4.13 Lower flange/endplate displacements with varying moments, M_z

The upper and lower flange have different displacements, the lower flange has a maximum displacement of approximately 4.5 mm, while the upper flange only displaces approximately 3.8 mm. It can be seen in figure 4.14, that the beam web displacement shows the degree of disproportion between the lower and upper beam flanges, in which

the endplate bends. The difference of the web ends stays the same for the last two time steps. For elastic limit 4.8 kNm not much displacements can be seen in the figure.

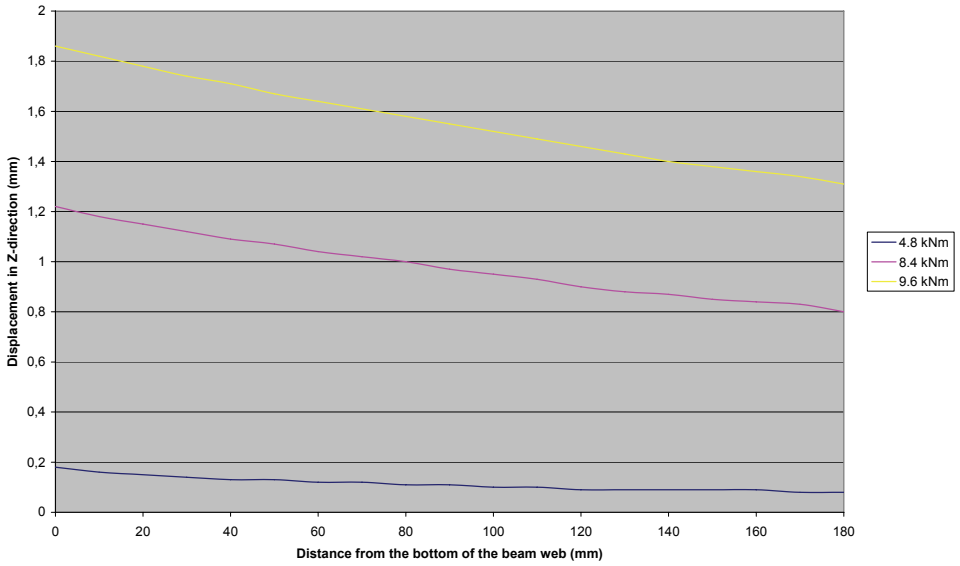

Figure 4.14 Beam web/endplate displacements with varying moments, M_z

The clear twisting of the beam might be the contributing factor on the simulation not achieving as high a collapse moment as the strong direction case. The upper flange is compressed more, and therefore the calculations overestimate the resistance on the compression side. The termination of the calculation presumably occurred when the element at upper compressed flange (compression component C6 in section 2.4) distorted. This can be seen in figure 4.15.

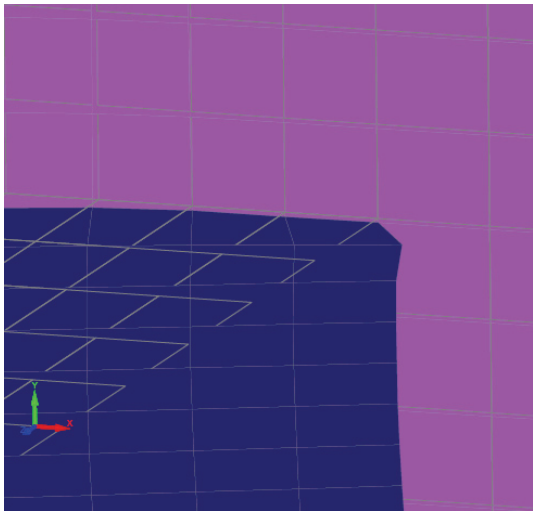

Figure 4.15 Detail picture of the distorted elements in the compressed flange (scale 2)

The upper end of the endplate was constrained in z-direction also in this case due to convergence problems, this might cause some error to the results, as the upper end of the endplate may not be in contact with the column for whole of its length.

However, more studies are needed in the future to a further test the application of component method for this case. The displacements of the beam flanged, visible in figures 4.13 and 4.14, indicate that the hypothesis of division of the compressed flanges to three equal parts (Heinisuo, Lehtimäki, Laine 2009) might be correct. In this simulation, however, the difference of the moment resistance, when compared to the component method calculation, was not sufficiently large for the weak axis bending. Also comparisons for the joint rotational stiffness is needed in further studies.

5. MODELLING OF THE WHOLE FRAME

5.1. Test Description

The simulations of experiments made by Wang et al (2008) were one scope of this study. The purpose of the experiments was to gain knowledge about joint robustness when subjected to fire, and to gain data to validate numerical models of joints. From the series of 10 tests, the test number 5 was selected for modelling in this study. The joint of the test 5 is presented in figure 5.1

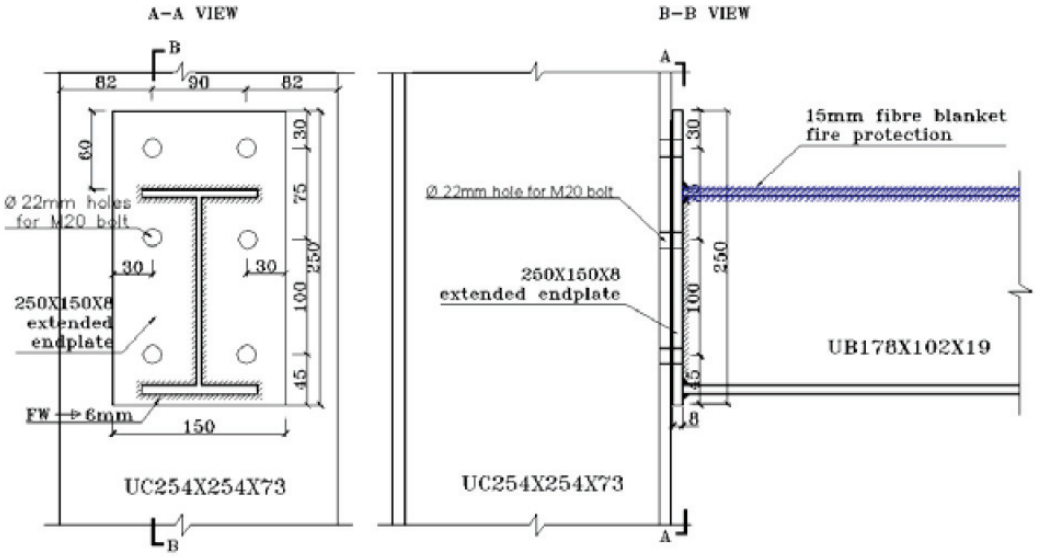

Figure 5.1 The joint of the test number 5 (Wang et al 2008)

The tests were done in a reaction frame and the whole setup was subjected to fire. Two 40 kN loads, corresponding 0.5 times the ultimate load of the beam, were implemented by two jacks and kept constant through the experiment.

The columns were only partially in the furnace, the exposed height being 900 mm. The column cross section was UC254 and beam cross section UB178. A schematic picture of the test setup is presented in figure 5.2.

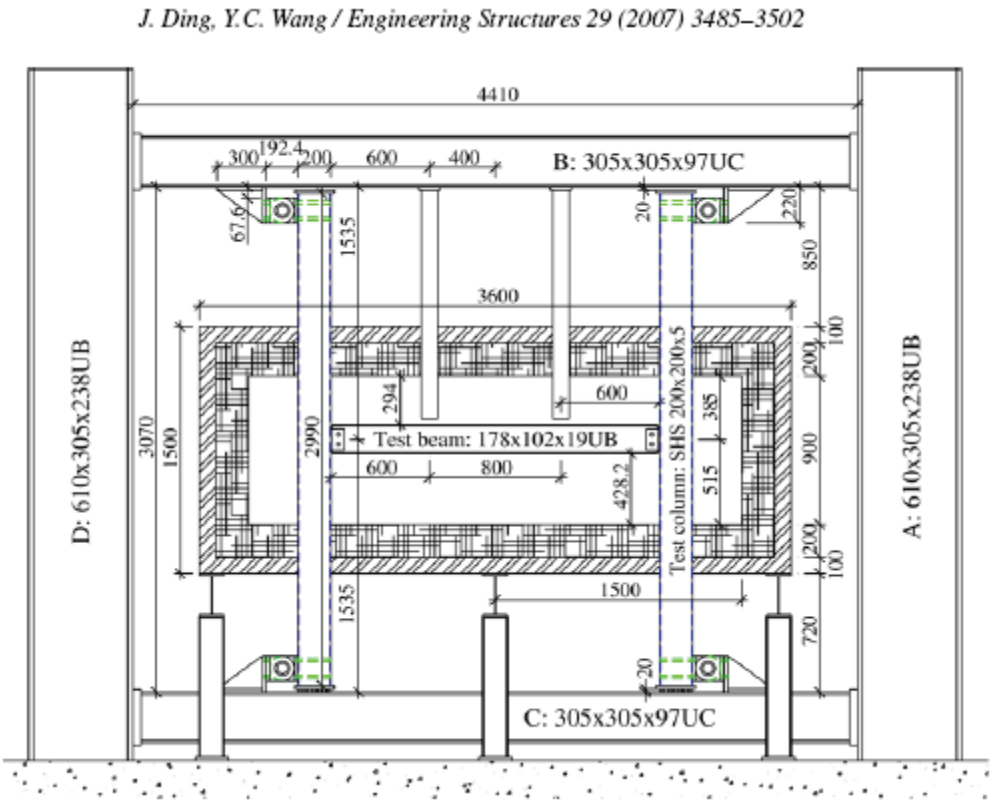

Figure 5.2 The test setup (Ding and Wang 2007)

It should be noted that figure 5.2 is not from the paper Wang et al (2008), but instead from an other test made by Ding and Wang (2007). Thus the column cross section in the figure is not correct. The ends of the columns were supported so that they may be considered pinned. The support in the upper end of the column allowed for the longitudinal movement of the column end. The supports are presented in figure 5.3.

Figure 5.3 The supports in the test (Wang et al 2008)

The total length of the column was 2990 mm. The length for modeling was taken from the halfway of the pins supporting the columns, giving length of 2790 mm. During the modeling this was somewhat shortened to the length of 2630 mm, due to time saving reasons.

For considering the effect of the constraining and heat sinking effect of concrete plate present in real life applications, the upper flange of the beam was insulated with a 15 mm thick resistant ceramic fiber blanket and a truss was built to prevent lateral torsional buckling of the beam, see fig 5.4 (Wang et al 2008). The truss was not modelled in this study.

Figure 5.4 The upper flange insulation and truss (Wang et al 2008)

The test was done until the displacement reached the maximum value possible with the test setup and had to be terminated. No fracture occurred during the test. The temperature when the test was terminated was approximately 725 ˚C. Details of the experiments and the results can be found in reference Wang et al (2008).

5.2. Model description

5.2.1. Geometry and Materials

The simple model described in chapter 4 was used as the base for modelling the frame. The endplate and the contacts were used as such in the frame model, with contact elements added also to the edges of the endplate. The beam length was increased to 0.992 meter. The column was made of shell elements by expanding the rigid foundation and changing its shell type. The mesh was coarser towards the end of the column. The total column length was 2630 mm. As the fire exposure is not along the whole of the column and SAFIR does not calculate heat transfer in longitudinal direction, the model required approximation when considering the heat. The heated area was increased to 1.2 meters, and the rest of the column was considered to be at the ambient temperature (20 ˚C). Ten different shell types were used to model the frame. The geometry and different shells are represented in figure 5.5. Thicker elements were placed to both ends of the column to prevent convergence problems at the support points.

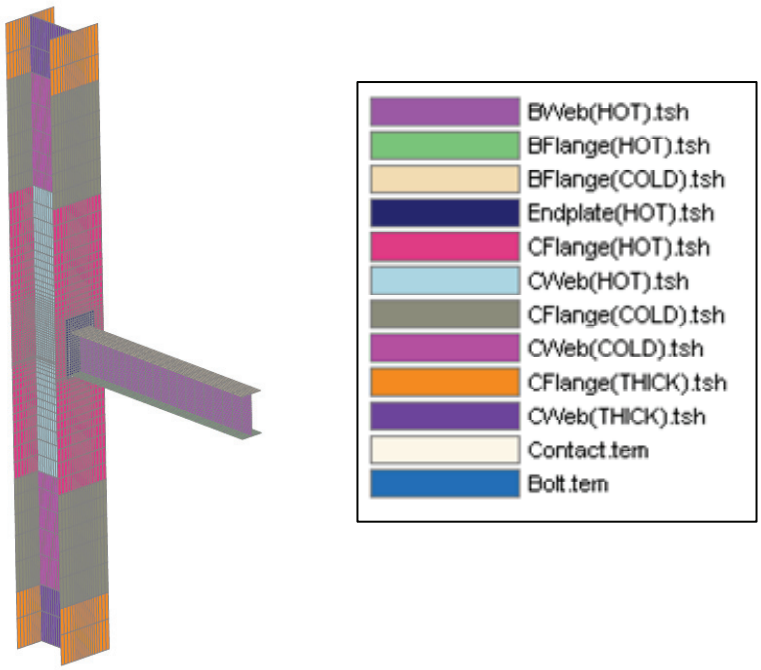

Figure 5.5 The geometric properties of the half frame model

In the test, a tension coupon test was also done to the tested beams. The result showed that the actual yield strength of the material was 345 instead of the nominal stress 275 MPa (Wang et al 2008). This value was used for calculations for S275 steel type of the beam, nominal strength was used for endplate as no tension coupon tests were done for the endplate steel. The column was of made steel S355, and the nominal yield strength of 355 MPa was used in the calculations.

The material and temperature properties for different cross section types presented in the legend of figure 5.5 are clarified in table 5.1. The truss section bolt.TEM and contact.TEM are the same as in chapter 4. All cross section types with HOT-definition attached to them are exposed to fire, the ones defined as COLD are in ambient temperature 20 °C. The thick column sections defined by THICK, are in ambient temperature. The mass of the shells were calculated using the volume mass of 7850 kg/m^3.

Table 5.1 The cross section thicknesses and yield stresses for .TSH-sections

Cross section type	Yield stress (Mpa)	Thickness (mm)
Bweb	345	5
Bflange	345	8
Cflange	355	14
Cweb	355	9
Endplate	275	8
CFlange(THICK)	355	140
Cweb(THICK)	355	90

5.2.2. Constraints

The column was restrained from both ends from the middle of the web. Both ends were made from thicker shells to prevent local failure of the column. The lower end was completely translationally constrained, and the upper end allowed movement in the Y-direction. The beam end was constrained from every node for every other displacement, except the translational movement to Y-direction, or down in this case. The global constraints of the frame are presented in figure 5.6.

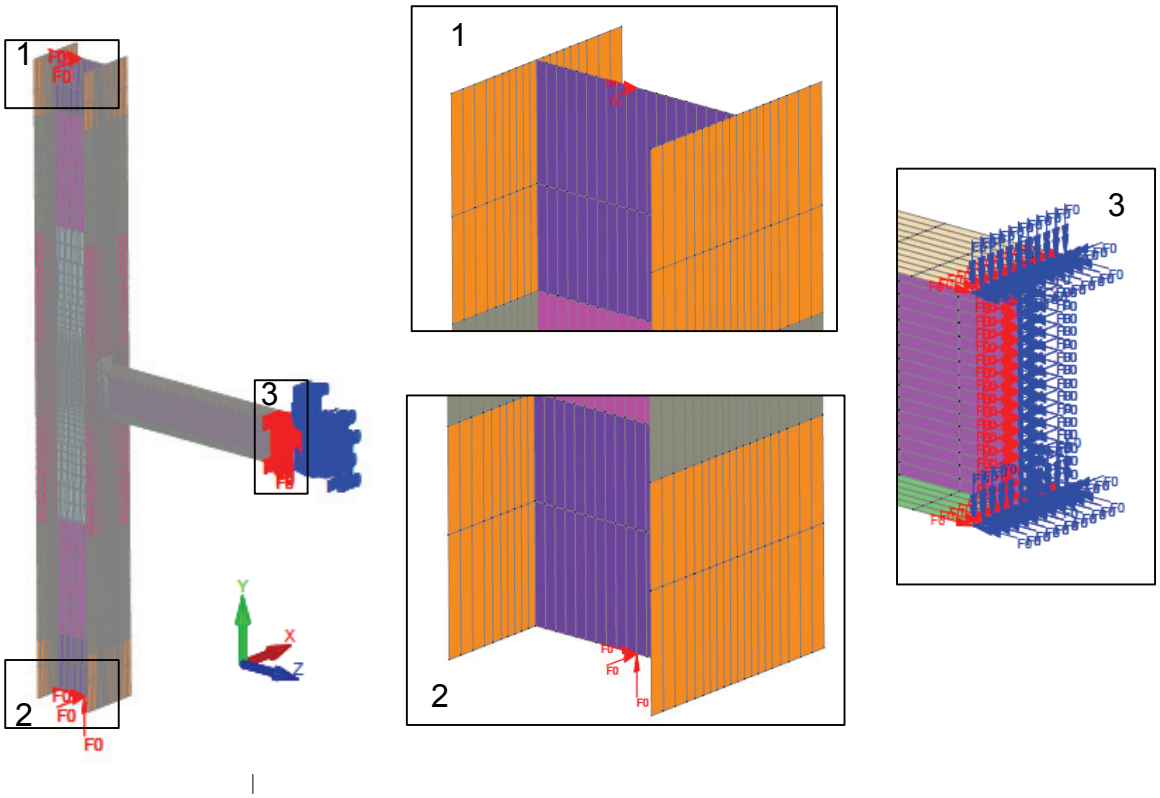

Figure 5.6 The boundary conditions for half frame model

The endplate was not absolutely constrained, but connected to the column by a slave-master relationship, in which the endplate was the master. The middle node of the lower end of the endplate was defined to have the same Y- and X-displacement with the column node opposite to it in Z-direction. Also at the lower end the corner nodes of the endplate were connected to the corresponding column nodes in Y-direction, see figure 5.7.

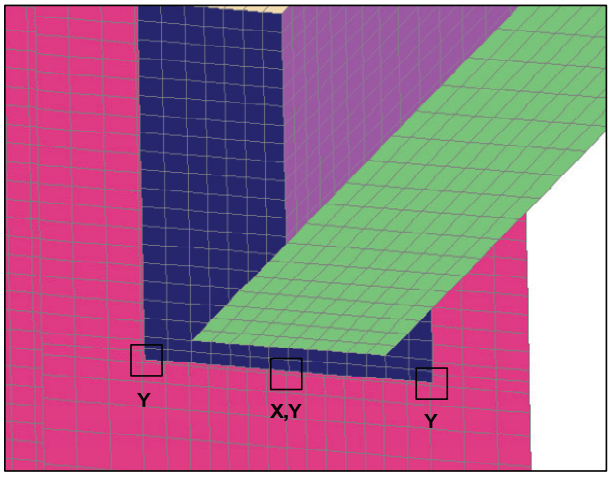

Figure 5.7 The master-slave connection in the lower end of endplate

The node at the middle of the upper end of the endplate was defined to have the same X-displacement with the opposite column node, see figure 5.8.

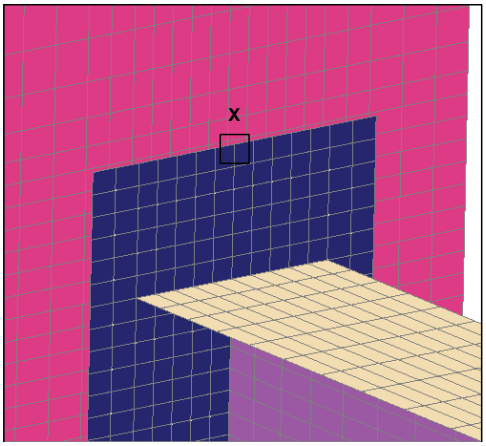

Figure 5.8 The master-slave connection in the upper end of endplate

5.2.3. Fire exposure

The fire exposure in the modelled tests followed the ISO 834 time - temperature fire curve (Franssen 2007). The curve for the first 90 minutes is plotted in figure 5.9. The curve is described by the equation $T = 20 + 345*LOG_{10}(8t+1)$, where t is time in minutes and T temperature in degrees Celsius. The insulating material present in the upper flange of the beam in the test was modeled so that the upper flange was considered to be in the ambient temperature 20 ˚C.

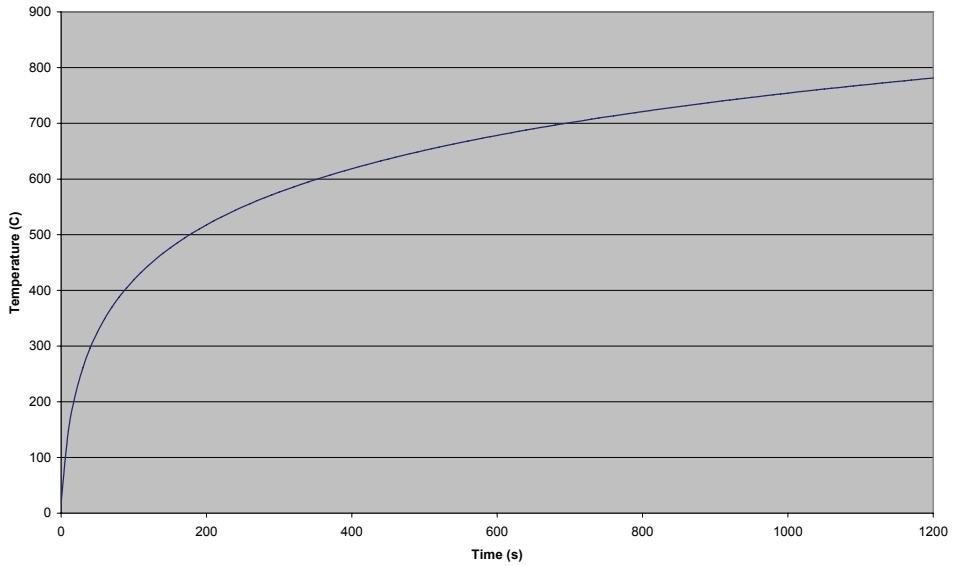

Figure 5.9 The ISO 834 time-temperature curve

5.2.4. Loading

The load was implemented as a point load to the node nearest to the loading jack in the test. The load was off by 110 mm from the test setup. The magnitude of the point load was 39.25 kN instead of 40 kN because of this. As the load is reasonably large, it had to be assigned incrementally, as the whole load was too much all at once. For step-by-step assignment of load function "FLOAD" was introduced. With "FLOAD" the function with which the load vector is multiplied is $t/20$ until $t = 20$, and 1 when $t > 20$. The loading curve is plotted in figure 5.10.

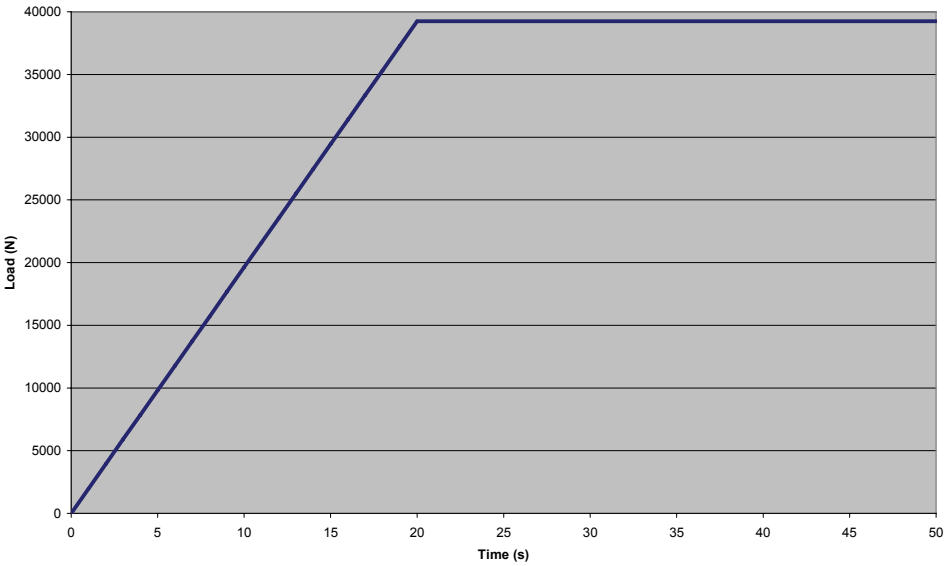

Figure 5.10 The load used in the half frame simulation

The temperature rise during the buildup of the load was not considered meaningful.

5.3. Results

The result from the half frame model presented here is the temperature at which the collapse of the beam initiated. The beam midpoint displacements from the test and from the simulation are presented in figure 5.10.

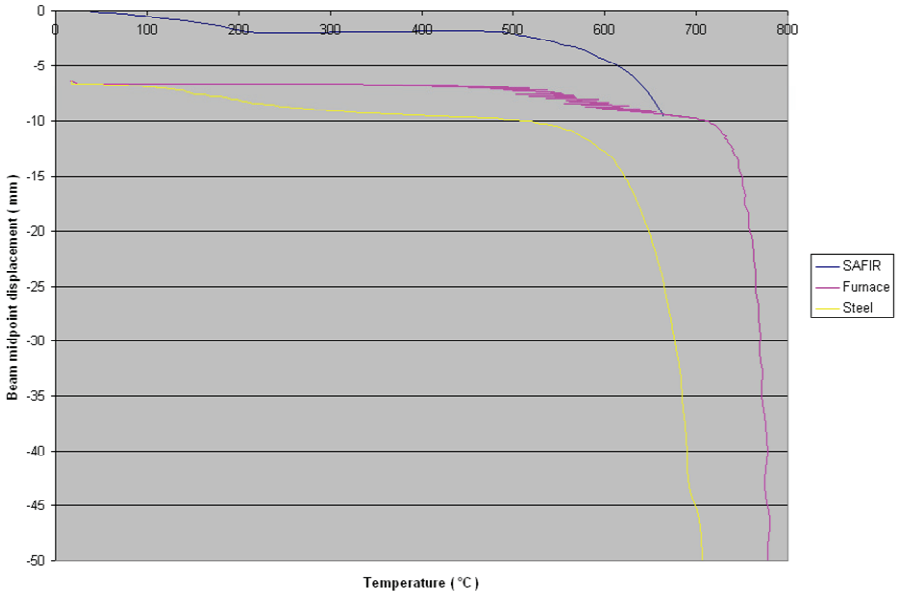

Figure 5.11 The beam midpoint displacements from test (Chen 2007) and simulation

A notable difference in the curves in figure 5.10 is the difference in the initial displacement. This is because of the different assignment of loading in the test. In the model it was implemented simultaneously with the fire exposure, while in test the load was already full when the furnace was turned on. However, there is still large difference in the initial displacement between the model and the test. The average temperature in the furnace at the initiation of collapse was approximately 750 °C, and in steel approximately 625 °C. The simulation reached the temperature of 660 °C before the displacement started to increase strongly. After the collapse initiated, the convergence was lost and calculation terminated. The temperature fits well between the two temperatures from the test, and the shape of the curve is the same as in the test, when the initial displacement difference is taken in to account.

Visual observations from the graphical post processing were also made. The whole model is presented in the figure 5.12 at the last time step. It can be seen that the displacements are small, and hard to notice with the scale factor 1. The column is undeformed. More detailed pictures will be presented next.

Figure 5.12 The half frame model at the last time step, scale1

The beam and endplate are plotted in figure 5.13, with scale factor 2.

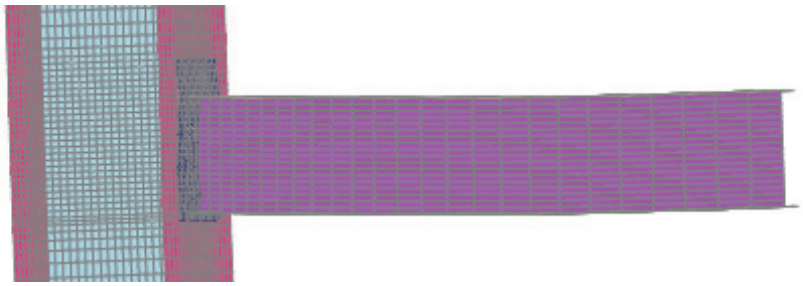

Figure 5.13 The endplate and beam at the last time step, scale 2

With scale factor 2 and closer picture some deformations are clearly visible. The column is still undeformed, which agrees with the test. There is a slight bend in the beam and the endplate has started to deform. The symmetrical boundary conditions at the beam end work as supposed. Endplate deformation is presented in figure 5.14.

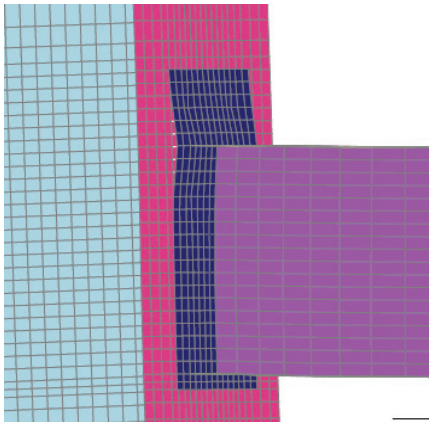

Figure 5.14 Endplate, scale 2

The probable cause for loss of convergence, the master slave relationship between endplate and the column, is presented in figure 5.15.

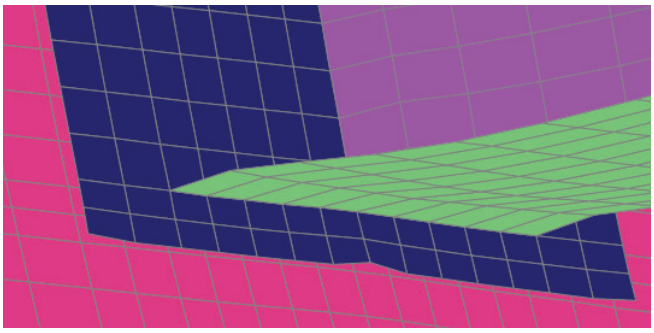

Figure 5.15 The distortion of lower end of endplate, scale 10

The scale in figure is large for visualization purpose, but the distortion of the elements connected to the constrained nodes is clear. The nodes were not constrained in Z-direction, in which the distortion is happening, the distortion is probably related to the contact elements used. Unfortunately there was not enough time to evaluate and fix this problem.

6. CONCLUSIONS

6.1. Results

6.1.1. Simple model

The model gave some new insight and data for evaluation and creating of 3D components. Some encouraging information regarding the weak axis bending component proposed in reference Heinisuo, Laine, Lehtimäki (2009) resulted from the weak axis bending case. More cases need to be modelled in the future to validify these results.

6.1.2. Half frame model

The model started to collapse at reasonably close to the temperatures in the tests. The model was promising, but did not fully succeed. It is however clear that this kind of simulation can, and should be, successfully done in the future.

6.2. Notes on Modeling and Sources of Error

6.2.1. Contact Elements

The main problem in this study was the lack of contact elements in SAFIR. This caused many unresolved convergence problems around the edges of the endplate, and these required the introduction of boundary conditions to such places, where their effect to the results of the simulation was uncertain. In the latter case, half frame from the test (Wang et al 2008), similar problems were met with the master-slave connection between the endplate and the column, causing distortion in the elements connected with the relationship, as seen in figure 5.14. The contacts were also strongly inclined in the latter parts of the simple model simulations, making their functionability questionable. Avoiding this inclination would have required large set of additional master – slave relationships.

6.2.2. Modelling of the Bolts by Trusses

The bolts were represented by truss elements in both simulations. This leads to highly concentrated point forces in the endplate and the column. This leads to stronger bending around the bolt in the shell element, than would be expected from more realistic bolt representations. The stiffness of the joint was low, resulting to large rotations. This can be at least partly attributed to the method of modeling the bolts. The bolts were also somewhat misplaced in the model due to the method of creating the mesh and time limitations. This misplacement, even if small, must be taken into account when evaluating

the results. Also the additional bending stiffness and bending resistance caused by bolts are missing when using this approach.

6.2.3. Lack of Welds in the Model

The welds were not modelled in SAFIR. This is more relevant for the half frame case, as the welds were also omitted from the calculations by the component method. The welds make the joint both stiffer and more resilient. The magnitude of the effect of leaving them out is uncertain.

6.2.4. The Heat Exposure

In the half frame model, the heat exposure for the different elements was the same for all of them. This is unrealistic, and leads to higher steel temperatures than would be expected in an experiment. The other end of this error is that the heat insulated upper flange was in ambient temperature during the whole test.

6.2.5. The Asymmetrical Bending

As the component calculation in section 2, for the weak moment case, did not take the asymmetrical bending into account, the compression resistance from the calculation may be overestimated. This is because the lower flange of the beam displaces more, as can seen in figure 4.15 , and supposedly causes the upper flange to be under more severe compression, when compared to the lower flange.

6.2.6. Interaction with GiD and SAFIR

As third party modelling software GiD was used in creating the model and the mesh, there is a possibility of some of the nodes being created in not an optimum way. This problem may be partly reason for the encountered convergence problems with the contact elements.

REFERENCES

Al-Jabri, K.S. 2000. The Behaviour of Steel and Composite Beam-to-Column connections in Fire. PhD Thesis, University of Sheffield.

Burgess, I.W. 2007. Connection modelling in fire. COST C26 Workshop: Urban habitat construction under catastrophic events, Prague, Czech Republic. pp 25-34.

Chen L. 2007. The source data for: An experimental study of fire behaviour and robustness of different types of steel joint in restrained steel frames, ASCE Journal of Structural Engineering (Wang, Dai, Bailey 2007), Spreadsheet data, Personal correspondence.

Ding, J., Wang, Y.C. 2007, Experimental study of structural fire behaviour of steel beam to concrete filled tubula column assemblies with different types of joints. Engineering structures, volume 29, number 12, December 2007, pp. 3485-3502.

EN-1992-1-1. 2005. Eurocode 2: Design of concrete structures, Part 1-1: General rules and rules for buildings. CEN, Brussels. 226 pages.

EN-1993-1-5. 2006. Eurocode 3: Design of steel structures, Part 1-5: Plated Structural Elements. CEN, Brussels. 54 pages.

EN-1993-1-8. 2005. Eurocode 3: Design of steel structures, Part 1-8: Design of joints. CEN, Brussels. 136 pages.

EN-1998-1. 2005. Eurocode 8: Design for earthquake resistance, Part 1 :General rules, seismic actions and rules for buildings. CEN, Brussels. 230 pages.

Fransen, J.M. 2007. Users manual for SAFIR 2007. University of Liege, Liege. 78 pages.

Franssen, J.M., Kodur, V.K.R., Mason, J. 2002. Elements of theory for SAFIR. University of Liege. Liege. 34 pages.

Heinisuo, M., Laine, V., Lehtimäki, E. 2009. Enlargement of the component method to 3D. Proceedings of Nordic steel conference, September 2-4, Malmö, Sweden. pp. 400 – 436.

NCSTAR 1-9. 2008. The structural fire response and the probable collapse sequence of world trade center 7. NIST.

Nethercot D.A., Zandonini R. 1989. Methods of prediction of joint behaviour: Beam-To-Column Connections, Stability and strength, ed. Narayanan R. Elsevier Applied science publishers, London. Pages 23 – 62.

Simoẽs Da Silva, L. 2008. Towards consistent design approach for steel joints under generalized loading. Journal of constructional Steel Research, Volume 64, Issue 9, Pages 1059-1075.

Tschemmernegg F., Tautschnig A., Klein H., Braun Ch., Humer Ch. 1987. Zur Nachgiebigkeit von Racmenknoten – Teil 1 (Semi-rigid joints of frame structures Vol. 1. – in german), Stahlbau 56, Heft 10, pages 229-306.

Wang, Y.C., Dai, X.H., Bailey, C.G. 2008. An experimental study of fire behaviour and robustness of different types of steel joint in restrained steel frames, ASCE Journal of Structural Engineering, Under Review. 27 pages.

Zoetemeijer, P. 1974. A design method for the tension side of statically loaded, bolted beam-to-column connections. Heron, Vol.20, no. 1. 59 pages.

APPENDIX 1: INPUT FILE FOR SIMPLE MODEL

Input file for simple model, strong direction moment.
Geometry greated by GiD.
NOTE: this is not a full input file, but a shortened example.
Removed segments are marked by "...".

```
     NNODE  2245
      NDIM    3
 NDIMMATER    1
   NDOFMAX    6
EVERY_NODE    6
       END_NDOF
   DYNAMIC   APPR_NR
   DAMPING  0.1
     NLOAD    1
   OBLIQUE    0
NOCOMEBACK
 LARGEUR11    400000
 LARGEUR12      1000
NORENUM
      NMAT    3
  ELEMENTS
     TRUSS    325     2
     SHELL   1488     6
   NGTHICK    3
    NGAREA    2
   NREBARS    0
  END_ELEM
     NODES
      NODE     1    0.0506   -0.0889    0.4000
      NODE     2    0.0405   -0.0889    0.4000
      NODE     3    0.0506   -0.0889    0.3800
      ...
      NODE  2243   -0.0750    0.1489    0.0000
      NODE  2244   -0.0628    0.1489   -0.0050
      NODE  2245   -0.0750    0.1489   -0.0050
 FIXATIONS
     BLOCK   762   NO   F0   NO   NO   NO   NO   NO
     BLOCK   770   NO   F0   NO   NO   NO   NO   NO
     BLOCK   771   NO   F0   NO   NO   NO   NO   NO
     ...
     BLOCK  2244   F0   F0   F0   F0   F0   F0   NO
     BLOCK  2245   F0   F0   F0   F0   F0   F0   NO
     BLOCK 1924 NO NO NO NO F0 F0
     SAMEALL YES YES YES NO NO NO
   END_FIX
NODOFSHELL
Endplate.tsh
 TRANSLATE    1    1
 END_TRANS
Foundation.tsh
 TRANSLATE    1    1
 END_TRANS
BLFlange.tsh
 TRANSLATE    1    1
 END_TRANS
BUFlange.tsh
 TRANSLATE    1    1
 END_TRANS
```

```
Web.tsh
 TRANSLATE    1    1
 END_TRANS
Web(THICK).tsh
 TRANSLATE    1    1
 END_TRANS
      ELEM     1   755   766   757   752     1
      ELEM     2   773   779   766   755     1
      ELEM     3   792   798   779   773     1
      ...
      ELEM  1486  1766  1827  1817  1757     2
      ELEM  1487  1817  1872  1867  1812     2
      ELEM  1488  1827  1885  1872  1817     2
NODOFTRUSS
Contact.tem           1.0000e-02 0.0000e+00    3
pultti.tem            2.78e-5  0.0000e+00    2
      ELEM     1  2227  2237     1
      ELEM     2  2201  2225     1
      ELEM     3  2157  2195     1
      ...
      ELEM   323   759   899     1
      ELEM   324   753   885     1
      ELEM   325   764   904     1
PRECISION 0.05
     LOADS
  FUNCTION        F1PS
 NODELOAD    246 0 -2000 0 0 0 0
  END_LOAD
      MASS
   M_SHELL     1 63.000000
   M_SHELL     2 63.000000
   M_SHELL     3 63.000000
   ...
   M_SHELL  1486 785.000000
   M_SHELL  1487 785.000000
   M_SHELL  1488 785.000000
  END_MASS
 MATERIALS
PLSTRVML
           210e+9   3.00e-01   2.75e+08 2.1e+9
BILIN
           210e+9   3.00e-01   9e+08 2.1e+9
SILCONC_EN
            3.00e-01   3.00e+07   0.00e+00
      TIME
       3.0     2400.0       36.0
  END_TIME
LARGEDISPL
     EPSTH
IMPRESSION
 TIMEPRINT
       3.0     2400.0
END_TIMEPR
 PRINTDEPL
  PRINTFHE
   PRINTMN
PRINTSHELL
PRNMXSHELL
```